

1 First response:

2
3 The material in this manuscript is suitable for publication in amt. It gives a useful com-
4 parison between an older particle probe, the 2DC, and the newer probe, the 2DS,
5 thought to provide more accurate ice crystal information. A compilation of the param-
6 eterization and normalization of many ice crystal size distributions measured by both
7 probe types is used in an attempt to adjust the older probe data to make that data more
8 reliable.

9
10 1. The paper needs a careful review concerning the lack of definition of some given
11 variables. For example, what is a a_{mi} and b_{mi} in Eq. (4), what is D_{eq} in the Figures,
12 what is subscript I ?

13
14 2. The accuracies of the density/dimension and mass/dimension relationships used in
15 the paper are not discussed, even though they may affect the conclusions reached. A
16 comment on such a possible affect.

17
18 3. The data for D05/D014 is listed as starting at 25 um; whereas the data for the 2DS
19 starts at 15 um. Is this taken into account in the comparisons?

20
21 4. The author points out the difficulty of the probes measuring the smallest ice crystals,
22 given that the probes can create errors due to uncorrected crystal shattering and other
23 reasons. His sentence associated with small crystals (line 181) “It is therefore felt that
24 the averaging approach is justified” is inconsistent with this difficulty.

25
26 5. The paper only deals with integrated ice-crystal properties, but it also points out that
27 the nature of the ice-crystal size distribution should also play a significant role in probe
28 performance. The latter is not dealt with in the paper. It would be helpful for the author
29 to comment on what might be done to improve the size information on the smallest
30 ice crystals that can dominate under certain atmospheric conditions (e.g., Heymsfield
31 et al., 2010, JAS, 67, 3303-3318). For example, can forward scattering probes that
32 respond to small particles be used for ice crystal measurements (e.g., Gerber and
33 DeMott, 2014, JTECH, 31, 2145-2155)?

34
35 6. The impressive Appendix is not essential for the conclusions reached in the paper.
36 Deletion of the Appendix is recommended.

37
38
39
40 **Response to Anonymous Referee #2**

41
42 Thank you for your thoughtful and helpful review. I will address your remarks in order.

43
44 1. This point is well taken. I have gone over the text and have removed inconsistencies (viz.,
45 that D_{eq} and D_e are supposed to be the same), have explicitly described each variable and its

46 subscript, and have removed the error of always using the letter “i” for every subscript. Rather
47 than document each change here, I’ve attached the marked-up manuscript to this reply.

48
49 2. In fact, there is an unfortunately high amount of uncertainty in these relations. It was felt that
50 the best that could be done was to use the same relations in this paper as in D05/D14 so as to
51 keep that part of the comparison consistent. This, of course, assumes the same overall mix of
52 particle habits was encountered between the PSD datasets. This is now noted in the discussion
53 section.

54
55 3. No, it is not. In light of the difference found, that is well worth pointing out and is done so in
56 the final section.

57
58 4. I think perhaps that I’ve not worded that sentence well and that it is redundant. The
59 “averaging approach” is adopted for smoothing out Poisson counting noise, not for ameliorating
60 measurement problems such as shattering. The shattered particle removal post-processing
61 (performed by the instrument team) is aimed at that. The sentence in question has been removed,
62 and the following sentence has been inserted at line 157 (given with the sentence prior for
63 context).

64
65 “In the first exercise, fifteen-second temporal averages were performed along with truncating
66 zero through two of the smallest size bins while only the unimodal fits (chosen according to a
67 maximum likelihood ratio test [Wilks, 2006]) were kept. This exercise was performed first so as
68 to prevent the most spurious size bins’ interfering with the smoothing out of Poisson counting
69 noise.”

70
71 5. This matter is now dealt with in the final section.

72
73 1) Finally, it is important to note that this study does not specifically consider PSD shape. (For a more
74 detailed discussion on cirrus PSD shape and on the efficacy of the gamma distribution, please refer to
75 Schwartz [2014].) This is a critical component of the answers to Korolov et al.’s (2013b) original two
76 questions. Mitchell et al. (2011) demonstrated that for a given effective diameter and IWC, the optical
77 properties of a PSD are sensitive to its shape. Therefore, PSD bimodality and concentrations of small ice
78 crystals are critical to realistically parameterizing, cirrus PSDs, to modeling their radiative properties and
79 sedimentation velocities, and to mathematical forward models designed to infer cirrus PSDs from remote
80 sensing observations (Lawson et al., 2010; Mitchell et al, 2011; Lawson, 2011). In order to improve
81 knowledge on PSD shape, as well as to develop statistical algorithms for correcting historical PSD datasets
82 so that PSD shapes are corrected along with computations of bulk properties, it will be necessary to make
83 use of instruments that can provide reliable measurements of small ice crystals beneath the size floors of
84 both the 2DC and the 2D-S. Recent studies such as Gerber and DeMott (2014) have provided aspherical

85 correction factors for particle volumes and effective diameters measured by the FSSP. However, the author
86 expects that this problem will ultimately be resolved by the continued technological development of new
87 probes such as the HOLODEC.

88
89
90 6. The Appendix has been removed.

91

92 Second response

93
94 **Response to Anonymous Referee #3**

95
96 I thank you for your thoughtful and helpful review. I will address your remarks (which are in
97 red) in order.

98
99
100 General Comments:

101 Overall the paper is suitable for publication with minor changes. The microphysical
102 probe comparisons presented are similar to past work, but the analyses are done in a
103 slightly different and more systematic way. My main comment is that the paper would
104 benefit from a more thorough introductory section, with historical insight into the probes
105 discussed and the characteristics that make them different. This should include not
106 only the ice shattering issue, but a brief summary of other technical differences.

107
108
109 Thank you! The following paragraphs have been added to the introduction.

110
111 While it is quite possible for relatively high numbers of small ice crystals to occur
112 naturally (see, e.g., Zhao et al., 2011; and Heymsfield et al., 2017), it is also possible for small
113 ice particle concentrations to be significantly inflated by several measurement artifacts. The
114 various particle size distribution (PSD) probes (also known as single particle detectors) in use
115 employ a handful of different measurement techniques to detect and size particles across a
116 variety of particle size ranges. The units of a PSD are number of particles per unit volume per
117 unit size. Thus, after a PSD probe counts the particles that pass through its sample area, each
118 particle is assigned a size as well as an estimate of the sample volume from which it was drawn
119 (Brenguier et al., 2013). Uncertainty in any of these PSD components results in uncertain PSD
120 estimates.

121 Leaving aside technologies still under development and test, such as the holographic
122 detector of clouds (HOLODEC; Fugal and Shaw, 2009), PSD probes fall into three basic
123 categories: impactor probes, light scattering probes, and imaging probes. (More thorough
124 discussions on this topic, along with comprehensive bibliographies, may be found in Brenguier
125 et al., 2013, and in Baumgardner et al., 2017.) The earliest cloud and precipitation particle
126 probes were of the impactor type (Brenguier et al., 2013). Modern examples include the Video
127 Ice Particle Sampler (VIPS) (Heymsfield and McFarquhar, 1996), designed to detect particles in
128 the range 5-200 μm . The basic operating principle is thus: cloud and precipitation particles
129 impact upon a substrate, leaving an imprint (or leaving the particle itself) to be replicated (in the
130 case of the VIPS, by digital imaging) and analyzed. This type of probe is particularly useful for
131 imaging the smallest ice crystals (Baumgardner et al., 2011; Brenguier et al., 2013).

132 Light scattering probes also are designed for detecting small, spherical and quasi-
133 spherical particles (a typical measurement range would be 1-50 μm ; see Baumgardner et al.,
134 2017). These work by measuring, at various angles, the scatter of the probe's laser due to the
135 presence of a particle within the probe's sample area. Assuming that detected particles are
136 spherical and assuming their index of refraction, Mie theory is then inverted to estimate particle

137 size. Two prominent examples of this type of probe are the Forward Scattering Spectrometer
138 Probe (FSSP; Knollenberg, 1976, 1981) and the Cloud Droplet Probe (CDP; Lance et al., 2010).

139 Imaging probes, also known as optical array probes (OAPs), use arrays of photodetectors
140 to make two-dimensional images of particles that pass through their sample areas. Unlike the
141 light scattering probes, OAPs make no assumptions regarding particle shape or composition
142 (Baumgardner et al., 2017), and they have broader measurement ranges aimed both at cloud and
143 precipitation particles. Two prominent examples are the Two-Dimensional Stereo (2D-S;
144 Lawson et al., 2006) probe, whose measurement range is 10-1280 μm , and the Two-Dimensional
145 Cloud (2DC; Knollenburg, 1976) probe, whose measurement range is 25-800 μm . OAPs
146 designed for precipitation particle imaging include the Precipitation Imaging Probe (PIP;
147 Baumgardner et al., 2001) and the High Volume Precipitation Spectrometer (HVPS; Lawson et
148 al., 1998), which measure particles ranging from $\sim 100 \mu\text{m}$ up to several millimeters.

149 Because an estimate of the sample volume from which a particle is drawn is a function of
150 the particle's size and assumes that the particle is spherical (Brenquier et al., 2013), all PSD
151 probes suffer from sample volume uncertainty. Estimated sample volumes from OAPs perforce
152 suffer from the problem of sizing aspherical particles from 2D images (see Fig 5-40, Brenquier et
153 al., 2013). Nonetheless, impactor and light scattering probes both suffer from much smaller
154 sample volumes than do OAPs (Brenquier et al., 2013; Baumgardner et al., 2017; Heymsfield et
155 al., 2017). Scattering probes, for example, need up to several times the sampling distance in
156 cloud as OAPs to produce a statistically significant PSD estimate (see Fig. 5-3, Brenquier et al,
157 2013).

158 The obvious difficulty in sizing small ice crystals with light scattering probes is the
159 application of Mie theory to nonspherical ice crystals. Probes such as the FSSP and CDP are
160 therefore prone to undersizing ice crystals (Baumgardner et al., 2011; Brenquier et al., 2013;
161 Baumgardner et al., 2017).

162 Imaging particles using an OAP requires no assumptions regarding particle shape or
163 composition, but sizing algorithms based on two-dimensional images are highly sensitive to
164 particle orientation (Brenquier et al., 2013). Other sizing uncertainties stem from imperfect
165 thresholds for significant occultation of photodiodes, the lack of an effective algorithm for
166 bringing out-of-focus ice particles into focus, and the use of statistical reconstructions of partially
167 imaged ice crystals that graze a probe's sample area (Brenquier et al., 2013; Baumgardner et al.,
168 2017).

169 Ideally, PSDs estimated using different probes would be stitched together in order to
170 provide a complete picture of the ice particle population, from micron-sized particles through
171 snowflakes (Brenquier et al., 2013). However, while data from VIPS, fast FSSP, and Small Ice
172 Detector-3 (SID-3; Ulanowski et al., 2014) probes are available to complement the OAP data
173 used in this study, none of them are used on account of sizing uncertainties stemming from their
174 small sample volumes and from spherical particle assumptions. The two publications wherewith
175 comparison is made in this paper also restricted their datasets to OAPs.

176
177
178
179 Minor Comments:

180 Lines 21-22: Without reading the paper, this sentence in the Abstract is confusing and
181 does not logically follow. Please clarify or simplify abstract.

183 Lines 21-22 have been changed to “This is done so that measurements of the same cloud
184 volumes from parameterized versions of the 2DC and 2D-S can be compared with one another.”

185
186 Line 44: Add Garrett et al.: Small, highly reflective ice crystals in low-latitude cirrus,
187 GRL 2003.

188
189 Garrett et al. (2003) has been referenced and remarked on as follows. “Garrett et al. (2003)
190 estimated that small ice crystals, with equivalent radii less than 30 microns, contributed in excess
191 of 90% of total shortwave extinction during the NASA Cirrus Regional Study of Tropical Anvils
192 and Cirrus Layers-Florida Area Cirrus Experiment (CRYSTAL-FACE).”

193
194 Line 72: “which results jibes” is awkward—please rephrase.

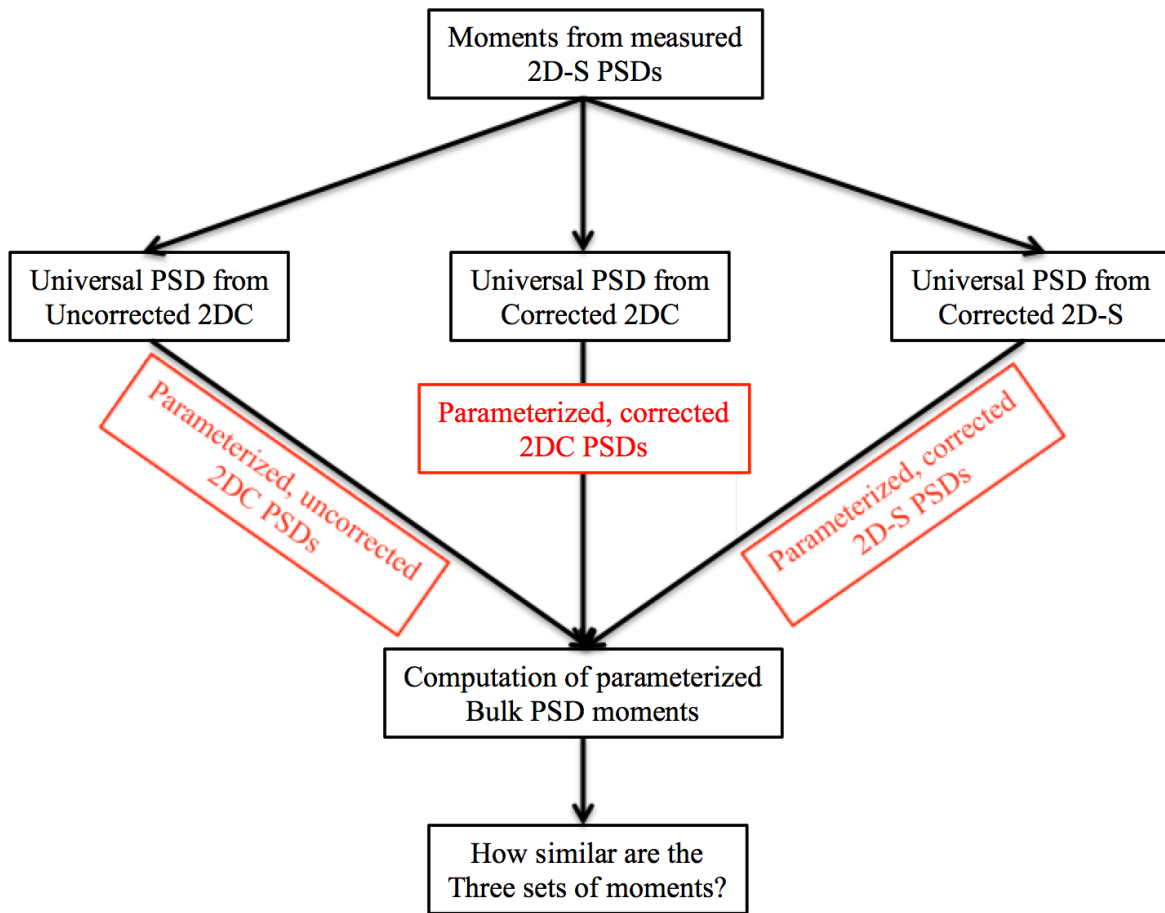
195
196 Line 72 rephrased to “in agreement with Lawson (2011)”.

197
198
199 Line 104-108: Perhaps a simple diagram would be helpful here to elucidate the method
200 and steps used?

201
202 The text has been changed to the following, and a new Figure 1 has been inserted as shown
203 below.

204
205 The comparison strategy, in short is as follows. The D05/D14 parameterizations consist of
206 normalized, “universal” cirrus PSDs to which PSD moments are applied as inputs. The results of
207 so doing are sets of parameterized 2DC PSDs—both shatter-corrected and uncorrected. To make
208 the comparison, the same moments from 2D-S-measured PSDs are applied to the D05/D14
209 parameterizations in order to simulate what the shatter- and non-shatter-corrected 2DCs would
210 have measured had they flown with the 2D-S. Then, a “universal” PSD derived from the 2D-S
211 itself is computed in order to make a fair comparison. The moments from the 2D-S-measured
212 PSDs are applied to the 2D-S “universal” PSD and it is then seen whether the older datasets
213 differ statistically from the newer in their derived cirrus bulk properties. This procedure is
214 illustrated in Fig. 1.

215



216
 217
 218
 219
 220
 221
 222
 223
 224
 225
 226
 227
 228
 229
 230
 231
 232
 233
 234
 235

Line 164: Why not use the actual size distributions?

The idea had been to see how the $\sim 2^{\text{nd}}$ moment of the fit PSD changed with varying degrees of truncation.

Line 166: Please quantify “nominally matches”, particularly since the data aren’t shown.

The word “nominally” has been replace with “qualitatively”.

Line 339: Is it really the “true” value?

No, I suppose not really the true values. The wording is changed to indicate that “true” means derived directly from the measurements.

Line 369: Missing subscript in NT. Corrected.

236
237
238
239
240
241
242
243
244
245
246
247
248
249
250
251
252
253
254
255
256
257
258
259
260
261
262
263
264
265
266
267
268
269
270
271
272
273

Line 376: Delete this sentence as it's not really necessary?

Redundant sentence deleted.

Lines 387: A long and wordy sentence. Suggest breaking it up for clarity.

Long sentence split apart.

Line 391: If your other work giving better alternatives to the Gamma distribution is now published, please refer to it here.

Unfortunately, this is still in the submission stage and not yet published. Therefore, a reference to my dissertation is inserted here.

Line 396-398: Redundant with statements in prior paragraph; remove.

Redundant statements have been deleted.

Acknowledgements: No acknowledgements to those scientists who provided the field data?

Thank you for pointing out this oversight. It has been corrected by inclusion of the following text.

The author gratefully acknowledges the SPartICus, MACPEX, and TC⁴ science teams for the collection of data used in this study. TC⁴ and MACPEX data were obtained from the NASA ESPO archive, which may be accessed online at <https://espoarchive.nasa.gov/archive/browse/>. The SPartICus data were obtained from DOE ARM archive and may be accessed online at <http://www.archive.arm.gov/discovery/#v/results/s/fiop::aaf2009Sparticus>. In particular, the author acknowledges Dr. Paul Lawson and SPEC, Inc. for all 2D-S data collected in the field, to Dr. Andrew Heymsfield for the PIP data used from TC⁴, and to Dr. Linnea Avallone for CLH data used from MACPEX.

274 Third response

275
276 Review: Minor revisions I agree with the previous reviewers in general. This is a pretty clean cut
277 topic for this paper which adds statistical consistency to a long standing problem in ice
278 measurement. Further, looking at the references, this is clearly one paper in a long series
279 originating with the author's days at Utah and beyond. While the topic is clean cut, the paper is
280 nevertheless difficult to follow at times, and the author could do much to improve readability,
281 and hopefully in time, his h-index. Indeed, it is overly terse at times. One previous reviewer
282 noted that the introduction could use a bit of background. I certainly concur with that. Even
283 though this has been reviewed in several other papers, it is good for a paper to be complete. Not
284 only to be tied in more completely with the previous literature base, but also with the author's
285 current lien of thought. I would also say the final results and discussion could also be worked on.
286 For example, the author states to the effect that old data is still usable, provided previously
287 described caveats are respected. Actually going through the paper several times, it was not clear
288 what all of these are. Even though the smaller ice sizes can be mitigated for the bulk moments,
289 what does this mean for say a forward optical model? Perhaps a separate conclusions, or
290 discussion and conclusions as distinct from results, be provided that provides a bulletined list of
291 what are the key take away points-sort of a recipe card. I would also suggest that figure captions
292 be more verbose spelling out variables when convenient. Similarly, laying out in a bulletining
293 form or table the different instruments and processing would help. Other than these comments,
294 my opinion matches those of the previous reviews: the paper oscillates between very formal
295 writing, and conversational vernacular(e.g., jibes, right off the bat, etc); a diagram laying out the
296 steps; . One point that requires emphasis as pointed out by reviewer 3 is the lack of data provider
297 documentation in the acknowledgements. Indeed, by downloading data from the NASA servers
298 not only did the author agree to acknowledge where the data came from, but actually offer
299 coauthor ship to the data providers. Often for this sort of thing they will simply ask for
300 acknowledgement, but the offer does need to be made. Be well.

301
302
303 **Response to Referee J. Reid**

304
305 I am grateful for your thoughtful review. I will attempt to address your remarks (in red) in order.

306
307 While the topic is clean cut, the paper is nevertheless difficult to follow at times, and the author
308 could do much to improve readability... Indeed, it is overly terse at times.

309
310 This point is well taken. I made a number of changes to make notation coherent and consistent
311 both within the text and within the figures, to make the tone more uniform, and to give better
312 explanations. Rather than document all of those changes here, I'll simply put the marked up
313 paper on with this reply.

314
315 One previous reviewer noted that the introduction could use a bit of background. I certainly
316 concur with that. Even though this has been reviewed in several other papers, it is good for a
317 paper to be complete. Not only to be tied in more completely with the previous literature base,
318 but also with the author's current lien of thought.

319

320 I fleshed out the literature review quite a bit and tried to provide more context. In so doing,
321 hopefully my own current line of thought is better fleshed out. The following paragraphs were
322 added to the introduction.

324 While it is quite possible for relatively high numbers of small ice crystals to occur
325 naturally (see, e.g., Zhao et al., 2011; and Heymsfield et al., 2017), it is also possible for small
326 ice particle concentrations to be significantly inflated by several measurement artifacts. The
327 various particle size distribution (PSD) probes (also known as single particle detectors) in use
328 employ a handful of different measurement techniques to detect and size particles across a
329 variety of particle size ranges. The units of a PSD are number of particles per unit volume per
330 unit size. Thus, after a PSD probe counts the particles that pass through its sample area, each
331 particle is assigned a size as well as an estimate of the sample volume from which it was drawn
332 (Brennguier et al., 2013). Uncertainty in any of these PSD components results in uncertain PSD
333 estimates.

334 Leaving aside technologies still under development and test, such as the holographic
335 detector of clouds (HOLODEC; Fugal and Shaw, 2009), PSD probes fall into three basic
336 categories: impactor probes, light scattering probes, and imaging probes. (More thorough
337 discussions on this topic, along with comprehensive bibliographies, may be found in Brennguier
338 et al., 2013, and in Baumgardner et al., 2017.) The earliest cloud and precipitation particle
339 probes were of the impactor type (Brennguier et al., 2013). Modern examples include the Video
340 Ice Particle Sampler (VIPS) (Heymsfield and McFarquhar, 1996), designed to detect particles in
341 the range 5-200 μm . The basic operating principle is thus: cloud and precipitation particles
342 impact upon a substrate, leaving an imprint (or leaving the particle itself) to be replicated (in the
343 case of the VIPS, by digital imaging) and analyzed. This type of probe is particularly useful for
344 imaging the smallest ice crystals (Baumgardner et al., 2011; Brennguier et al., 2013).

345 Light scattering probes also are designed for detecting small, spherical and quasi-
346 spherical particles (a typical measurement range would be 1-50 μm ; see Baumgardner et al.,
347 2017). These work by measuring, at various angles, the scatter of the probe's laser due to the
348 presence of a particle within the probe's sample area. Assuming that detected particles are
349 spherical and assuming their index of refraction, Mie theory is then inverted to estimate particle
350 size. Two prominent examples of this type of probe are the Forward Scattering Spectrometer
351 Probe (FSSP; Knollenberg, 1976, 1981) and the Cloud Droplet Probe (CDP; Lance et al., 2010).

352 Imaging probes, also known as optical array probes (OAPs), use arrays of photodetectors
353 to make two-dimensional images of particles that pass through their sample areas. Unlike the
354 light scattering probes, OAPs make no assumptions regarding particle shape or composition
355 (Baumgardner et al., 2017), and they have broader measurement ranges aimed both at cloud and
356 precipitation particles. Two prominent examples are the Two-Dimensional Stereo (2D-S;
357 Lawson et al., 2006) probe, whose measurement range is 10-1280 μm , and the Two-Dimensional
358 Cloud (2DC; Knollenburg, 1976) probe, whose measurement range is 25-800 μm . OAPs
359 designed for precipitation particle imaging include the Precipitation Imaging Probe (PIP;
360 Baumgardner et al., 2001) and the High Volume Precipitation Spectrometer (HVPS; Lawson et
361 al., 1998), which measure particles ranging from $\sim 100 \mu\text{m}$ up to several millimeters.

362 Because an estimate of the sample volume from which a particle is drawn is a function of
363 the particle's size and assumes that the particle is spherical (Brennguier et al., 2013), all PSD
364 probes suffer from sample volume uncertainty. Estimated sample volumes from OAPs perforce
365 suffer from the problem of sizing aspherical particles from 2D images (see Fig 5-40, Brennguier et

366 al., 2013). Nonetheless, impactor and light scattering probes both suffer from much smaller
367 sample volumes than do OAPs (Brenguier et al., 2013; Baumgardner et al., 2017; Heymsfield et
368 al., 2017). Scattering probes, for example, need up to several times the sampling distance in
369 cloud as OAPs to produce a statistically significant PSD estimate (see Fig. 5-3, Brenguier et al,
370 2013).

371 The obvious difficulty in sizing small ice crystals with light scattering probes is the
372 application of Mie theory to nonspherical ice crystals. Probes such as the FSSP and CDP are
373 therefore prone to undersizing ice crystals (Baumgardner et al., 2011; Brenguier et al., 2013;
374 Baumgardner et al., 2017).

375 Imaging particles using an OAP requires no assumptions regarding particle shape or
376 composition, but sizing algorithms based on two-dimensional images are highly sensitive to
377 particle orientation (Brenguier et al., 2013). Other sizing uncertainties stem from imperfect
378 thresholds for significant occultation of photodiodes, the lack of an effective algorithm for
379 bringing out-of-focus ice particles into focus, and the use of statistical reconstructions of partially
380 imaged ice crystals that graze a probe’s sample area (Brenguier et al., 2013; Baumgardner et al.,
381 2017).

382 Ideally, PSDs estimated using different probes would be stitched together in order to
383 provide a complete picture of the ice particle population, from micron-sized particles through
384 snowflakes (Brenguier et al., 2013). However, while data from VIPS, fast FSSP, and Small Ice
385 Detector-3 (SID-3; Ulanowski et al., 2014) probes are available to complement the OAP data
386 used in this study, none of them are used on account of sizing uncertainties stemming from their
387 small sample volumes and from spherical particle assumptions. The two publications wherewith
388 comparison is made in this paper also restricted their datasets to OAPs.

389 ... a diagram laying out the steps...

391
392 I put in improved text (below) about the steps and an accompanying figure (see the marked up
393 draft).

394
395 The comparison strategy, in short is as follows. The D05/D14 parameterizations consist of
396 normalized, “universal” cirrus PSDs to which PSD moments are applied as inputs. The results of
397 so doing are sets of parameterized 2DC PSDs—both shatter-corrected and uncorrected. To make
398 the comparison, the same moments from 2D-S-measured PSDs are applied to the D05/D14
399 parameterizations in order to simulate what the shatter- and non-shatter-corrected 2DCs would
400 have measured had they flown with the 2D-S. Then, a “universal” PSD derived from the 2D-S
401 itself is computed in order to make a fair comparison. The moments from the 2D-S-measured
402 PSDs are applied to the 2D-S “universal” PSD and it is then seen whether the older datasets
403 differ statistically from the newer in their derived cirrus bulk properties. This procedure is
404 illustrated in Fig. 1.

405
406 I would also say the final results and discussion could also be worked on. For example, the
407 author states to the effect that old data is still usable, provided previously described caveats are
408 respected. Actually going through the paper several times, it was not clear what all of these are.
409 Even though the smaller ice sizes can be mitigated for the bulk moments, what does this mean
410 for say a forward optical model? Perhaps a separate conclusions, or discussion and conclusions

411 as distinct from results, be provided that provides a bulletined list of what are the key take away
412 points-sort of a recipe card.

413
414 I've cleaned up the last section as well, summarizing the final points in a bulletined list as
415 suggested. I'll refer you to the attached revision for a discussion on psd shape and optical
416 models.

417
418 One point that requires emphasis as pointed out by reviewer 3 is the lack of data provider
419 documentation in the acknowledgements. Indeed, by downloading data from the NASA servers
420 not only did the author agree to acknowledge where the data came from, but actually offer
421 coauthor ship to the data providers. Often for this sort of thing they will simply ask for
422 acknowledgement, but the offer does need to be made.

423
424 You are quite correct about the acknowledgements. Co-authorship was offered to the data
425 providers, which was declined. Thank you for pointing out my oversight in not including the
426 data sources in the acknowledgements. References to the data sources are also given.

427
428

429 Fourth Response

430

431 **Response to Darrell Baumgardner**

432

433 This study is a logical and complementary follow-up of the Delanoë et al. (2005,2014)
434 evaluations that provided parameterizations of cirrus size distributions based on a large set of
435 measurements taken in both mid-latitude and tropical environments. The author has provided a
436 detailed analysis using more recent measurements with a more modern imaging probe to address
437 an important question: "Given what we now know about the impact of crystal shattering on
438 measurements by cloud particle spectrometers, can historical data sets be trusted"? I think that
439 this study has answered that question, at least with respect to cirrus clouds. In addition, even
440 though the instrument that is used in this study has a faster response time than the earlier 2D-C
441 and 2D-P, and marginally larger sample volume, the results of the current study would suggest
442 that such instrument improvements really have minor impact on the overall statistical robustness
443 of the previous measurements and may also only be marginally more accurate, especially given
444 the many other uncertainties that the new instrument has not overcome. In particular, there
445 remain major uncertainties due to unknown ice density and shape in the third dimension that lead
446 to large error bars in derived bulk parameters. It is only at the very smallest sizes where there is a
447 clear difference between current and previous measurements; however, even when there are
448 several orders of magnitude difference in concentration at these sizes, the propagated error in
449 effective radius, IWC and reflectivity is surprisingly small. What I think would be a useful, and
450 perhaps even necessary, addition to this paper would be to include in Figs. 7&8 the relative
451 errors and standard deviations that are reported in Delanoë et al. (2005,2014) where they
452 compare their data sets against the parameterization. That would then put into context the current
453 comparison with the parameterizations with the original, hence bringing closure. The other very
454 important source of uncertainty that the author side steps is that of oversizing of out-of-focus ice
455 crystals (Korolev, 2007). Although a correction for this issue has not yet been provided, such as
456 has been done for water droplets, measurements in cirrus clearly show crystal images that are out
457 of focus and that should be sizecorrected. These might even be the source of the "bump" in the
458 size distributions, i.e. a certain fraction of the particles in that size interval most certainly are
459 smaller crystals out of focus. This bump is also seen in the Delanoë et al. (2005,2014) studies;
460 however, whereas the bump occurs in the current study at a $Deq/DM < 1$, in Delanoë et al.
461 (2005,2014) the bump is right at 1. How does the author explain this? Lastly, the author refers
462 to three of his papers that have not yet been published. These references should be removed
463 since, as a reviewer, I was unable to access them.

464

465

466 I thank you for your time in providing a thoughtful review. I will attempt to address your
467 remarks (in red) in order.

468

469 What I think would be a useful, and perhaps even necessary, addition to this paper would be to
470 include in Figs. 7&8 the relative errors and standard deviations that are reported in Delanoë et al.
471 (2005,2014) where they compare their data sets against the parameterization.

472

473 I must confess that I entirely misread this comment at first and added error bars to show standard
474 error in the means and standard deviations to those figures. However, now that I have overcome

475 my stupor of thought and understand your comment correctly, I'm not sure that I can read the
476 numbers off those charts accurately enough to replot them.

477
478 The other very important source of uncertainty that the author side steps is that of oversizing of
479 out-of-focus ice crystals (Korolev, 2007). Although a correction for this issue has not yet been
480 provided, such as has been done for water droplets, measurements in cirrus clearly show crystal
481 images that are out of focus and that should be sizecorrected. These might even be the source of
482 the "bump" in the size distributions, i.e. a certain fraction of the particles in that size interval
483 most certainly are smaller crystals out of focus. This bump is also seen in the Delanoë et al.
484 (2005,2014) studies; however, whereas the bump occurs in the current study at a Deq/DM <1, in
485 Delanoë et al. (2005,2014) the bump is right at 1. How does the author explain this?

486
487 I have remarked on the out-of-focus problem in the revamped introduction. However, I have no
488 good explanation for the shifting of the bump. I decided to leave that unaddressed rather than
489 risk proffering a bad explanation. The additional text in the introduction follows.

490
491 While it is quite possible for relatively high numbers of small ice crystals to occur naturally (see, e.g., Zhao
492 et al., 2011; and Heymsfield et al., 2017), it is also possible for small ice particle concentrations to be significantly
493 inflated by several measurement artifacts. The various particle size distribution (PSD) probes (also known as single
494 particle detectors) in use employ a handful of different measurement techniques to detect and size particles across a
495 variety of particle size ranges. The units of a PSD are number of particles per unit volume per unit size. Thus, after
496 a PSD probe counts the particles that pass through its sample area, each particle is assigned a size as well as an
497 estimate of the sample volume from which it was drawn (Brennguier et al., 2013). Uncertainty in any of these PSD
498 components results in uncertain PSD estimates.

499 Leaving aside technologies still under development and test, such as the holographic detector of clouds
500 (HOLODEC; Fugal and Shaw, 2009), PSD probes fall into three basic categories: impactor probes, light scattering
501 probes, and imaging probes. (More thorough discussions on this topic, along with comprehensive bibliographies,
502 may be found in Brennguier et al., 2013, and in Baumgardner et al., 2017.) The earliest cloud and precipitation
503 particle probes were of the impactor type (Brennguier et al., 2013). Modern examples include the Video Ice Particle
504 Sampler (VIPS) (Heymsfield and McFarquhar, 1996), designed to detect particles in the range 5-200 μm . The basic
505 operating principle is thus: cloud and precipitation particles impact upon a substrate, leaving an imprint (or leaving
506 the particle itself) to be replicated (in the case of the VIPS, by digital imaging) and analyzed. This type of probe is
507 particularly useful for imaging the smallest ice crystals (Baumgardner et al., 2011; Brennguier et al., 2013).

508 Light scattering probes also are designed for detecting small, spherical and quasi-spherical particles (a
509 typical measurement range would be 1-50 μm ; see Baumgardner et al., 2017). These work by measuring, at various
510 angles, the scatter of the probe's laser due to the presence of a particle within the probe's sample area. Assuming
511 that detected particles are spherical and assuming their index of refraction, Mie theory is then inverted to estimate
512 particle size. Two prominent examples of this type of probe are the Forward Scattering Spectrometer Probe (FSSP;
513 Knollenberg, 1976, 1981) and the Cloud Droplet Probe (CDP; Lance et al., 2010).

514 Imaging probes, also known as optical array probes (OAPs), use arrays of photodetectors to make two-
515 dimensional images of particles that pass through their sample areas. Unlike the light scattering probes, OAPs make
516 no assumptions regarding particle shape or composition (Baumgardner et al., 2017), and they have broader
517 measurement ranges aimed both at cloud and precipitation particles. Two prominent examples are the Two-
518 Dimensional Stereo (2D-S; Lawson et al., 2006) probe, whose measurement range is 10-1280 μm , and the Two-
519 Dimensional Cloud (2DC; Knollenburg, 1976) probe, whose measurement range is 25-800 μm . OAPs designed for
520 precipitation particle imaging include the Precipitation Imaging Probe (PIP; Baumgardner et al., 2001) and the High
521 Volume Precipitation Spectrometer (HVPS; Lawson et al., 1998), which measure particles ranging from $\sim 100 \mu\text{m}$
522 up to several millimeters.

523 Because an estimate of the sample volume from which a particle is drawn is a function of the particle's size
524 and assumes that the particle is spherical (Brennguier et al., 2013), all PSD probes suffer from sample volume
525 uncertainty. Estimated sample volumes from OAPs perforce suffer from the problem of sizing aspherical particles
526 from 2D images (see Fig 5-40, Brennguier et al., 2013). Nonetheless, impactor and light scattering probes both suffer

527 from much smaller sample volumes than do OAPs (Brenguier et al., 2013; Baumgardner et al., 2017; Heymsfield et
528 al., 2017). Scattering probes, for example, need up to several times the sampling distance in cloud as OAPs to
529 produce a statistically significant PSD estimate (see Fig. 5-3, Brenguier et al, 2013).

530 The obvious difficulty in sizing small ice crystals with light scattering probes is the application of Mie
531 theory to nonspherical ice crystals. Probes such as the FSSP and CDP are therefore prone to undersizing ice crystals
532 (Baumgardner et al., 2011; Brenguier et al., 2013; Baumgardner et al., 2017).

533 Imaging particles using an OAP requires no assumptions regarding particle shape or composition, but
534 sizing algorithms based on two-dimensional images are highly sensitive to particle orientation (Brenguier et al.,
535 2013). Other sizing uncertainties stem from imperfect thresholds for significant occultation of photodiodes, the lack
536 of an effective algorithm for bringing out-of-focus ice particles into focus, and the use of statistical reconstructions
537 of partially imaged ice crystals that graze a probe's sample area (Brenguier et al., 2013; Baumgardner et al., 2017).

538 Ideally, PSDs estimated using different probes would be stitched together in order to provide a complete
539 picture of the ice particle population, from micron-sized particles through snowflakes (Brenguier et al., 2013).
540 However, while data from VIPS, fast FSSP, and Small Ice Detector-3 (SID-3; Ulanowski et al., 2014) probes are
541 available to complement the OAP data used in this study, none of them are used on account of sizing uncertainties
542 stemming from their small sample volumes and from spherical particle assumptions. The two publications
543 wherewith comparison is made in this paper also restricted their datasets to OAPs.

544
545 Lastly, the author refers to three of his papers that have not yet been published. These references
546 should be removed since, as a reviewer, I was unable to access them.

547
548 I removed them and replaced them with a simple reference to my dissertation.

549
550
551
552
553

554

555

556 **A Statistical Comparison of Cirrus Particle Size Distributions**
557 **Measured Using the 2D Stereo Probe During the TC⁴,**
558 **SPartICus, and MACPEX Flight Campaigns with Historical**
559 **Cirrus Datasets**

560

561 M. Christian Schwartz

562 Argonne National Laboratory, 9700 Cass Avenue, Bldg. 240, 6.A.15, Lemont, IL, 60439, United States

563

564 *Correspondence to:* M. Christian Schwartz (mcs45@byu.net)

565 **Abstract.** This paper addresses two straightforward questions. First, how similar are the statistics of cirrus particle
566 size distribution (PSD) datasets collected using the 2D Stereo (2D-S) probe to cirrus PSD datasets collected using
567 older Particle Measuring Systems (PMS) 2D Cloud (2DC) and 2D Precipitation (2DP) probes? Second, how similar
568 are the datasets when shatter-correcting post-processing is applied to the 2DC datasets? To answer these questions,
569 a database of measured and parameterized cirrus PSDs, constructed from measurements taken during the Small
570 Particles in Cirrus (SPartICus), Mid-latitude Airborne Cirrus Properties Experiment (MACPEX), and Tropical
571 Composition, Cloud, and Climate Coupling (TC⁴) flight campaigns is used.

572 Bulk cloud quantities are computed from the 2D-S database in three ways: first, directly from the 2D-S
573 data; second, by applying the 2D-S data to ice PSD parameterizations developed using sets of cirrus measurements
574 collected using the older PMS probes; and third, by applying the 2D-S data to a similar parameterization developed
575 using the 2D-S data itself. This is done so that measurements of the same cloud volumes by parameterized versions
576 of the 2DC and 2D-S can be compared with one another. It is thereby seen, given the same cloud field and given the
577 same assumptions concerning ice crystal cross-sectional area, density, and radar cross section, that the parameterized
578 2D-S and the parameterized 2DC predict similar distributions of inferred shortwave extinction coefficient, ice water
579 content, and 94 GHz radar reflectivity. However, the parameterization of the 2DC based on uncorrected data
580 predicts a statistically significant higher number of total ice crystals and a larger ratio of small ice crystals to large
581 ice crystals than does the parameterized 2D-S. The 2DC parameterization based on shatter-corrected data also
582 predicts statistically different numbers of ice crystals than does the parameterized 2D-S, but the comparison between
583 the two is nevertheless more favorable. It is concluded that the older data sets continue to be useful for scientific
584 purposes, with certain caveats, and that continuing field investigations of cirrus with more modern probes is
585 desirable.

586 1 Introduction

587 For decades, in situ ice cloud particle measurements have often indicated ubiquitous, high concentrations of
588 the smallest ice particles (Korolev et al., 2013a; Korolev and Field, 2015). If the smallest ice particles are indeed
589 always present in such large numbers, then their effects on cloud microphysical and radiative properties are
590 pronounced. For instance, Heymsfield et al. (2002) reported small particles' dominating total particle concentrations
591 (N_{TS}) at all times during multiple Tropical Rainfall Measuring Mission (TRMM) field campaigns, while Field
592 (2000) noted the same phenomenon in mid-latitude cirrus. Lawson et al. (2006) reported N_{TS} in mid-latitude cirrus
593 ranging from $\sim .2$ - 1 cm^{-3} and estimated that particles smaller than 50 microns were responsible for 99% of N_T , 69%
594 of shortwave extinction, and 40% of ice water content (IWC). From several representative cirrus cases, Gayet et al.
595 (2002) reported average N_{TS} as high as 10 cm^{-3} and estimated that particles having maximum dimensions smaller
596 than 15.8 microns resulted in about 38% of measured shortwave extinction; and Gayet et al. (2004) and Gayet et al.
597 (2006) estimated from a broader set of measurements that particles smaller than 20 microns accounted for about
598 35% of observed shortwave extinction. Garrett et al. (2003) estimated that small ice crystals, with equivalent radii
599 less than 30 microns, contributed in excess of 90% of total shortwave extinction during the NASA Cirrus Regional
600 Study of Tropical Anvils and Cirrus Layers-Florida Area Cirrus Experiment (CRYSTAL-FACE).

601 While it is quite possible for relatively high numbers of small ice crystals to occur naturally (see, e.g., Zhao
602 et al., 2011; and Heymsfield et al., 2017), it is also possible for small ice particle concentrations to be significantly
603 inflated by several measurement artifacts. The various particle size distribution (PSD) probes (also known as single
604 particle detectors) in use employ a handful of different measurement techniques to detect and size particles across a
605 variety of particle size ranges. The units of a PSD are number of particles per unit volume per unit size. Thus, after
606 a PSD probe counts the particles that pass through its sample area, each particle is assigned a size as well as an
607 estimate of the sample volume from which it was drawn (Brennguier et al., 2013). Uncertainty in any of these PSD
608 components results in uncertain PSD estimates.

609 Leaving aside technologies still under development and test, such as the holographic detector of clouds
610 (HOLODEC; Fugal and Shaw, 2009), PSD probes fall into three basic categories: impactor probes, light scattering
611 probes, and imaging probes. (More thorough discussions on this topic, along with comprehensive bibliographies,
612 may be found in Brennguier et al., 2013, and in Baumgardner et al., 2017.) The earliest cloud and precipitation
613 particle probes were of the impactor type (Brennguier et al., 2013). Modern examples include the Video Ice Particle

614 Sampler (VIPS) (Heymsfield and McFarquhar, 1996), designed to detect particles in the range 5-200 μm . The basic
615 operating principle is thus: cloud and precipitation particles impact upon a substrate, leaving an imprint (or leaving
616 the particle itself) to be replicated (in the case of the VIPS, by digital imaging) and analyzed. This type of probe is
617 particularly useful for imaging the smallest ice crystals (Baumgardner et al., 2011; Brenguier et al., 2013).

618 Light scattering probes also are designed for detecting small, spherical and quasi-spherical particles (a
619 typical measurement range would be 1-50 μm ; see Baumgardner et al., 2017). These work by measuring, at various
620 angles, the scatter of the probe's laser due to the presence of a particle within the probe's sample area. Assuming
621 that detected particles are spherical and assuming their index of refraction, Mie theory is then inverted to estimate
622 particle size. Two prominent examples of this type of probe are the Forward Scattering Spectrometer Probe (FSSP;
623 Knollenberg, 1976, 1981) and the Cloud Droplet Probe (CDP; Lance et al., 2010).

624 Imaging probes, also known as optical array probes (OAPs), use arrays of photodetectors to make two-
625 dimensional images of particles that pass through their sample areas. Unlike the light scattering probes, OAPs make
626 no assumptions regarding particle shape or composition (Baumgardner et al., 2017), and they have broader
627 measurement ranges aimed both at cloud and precipitation particles. Two prominent examples are the Two-
628 Dimensional Stereo (2D-S; Lawson et al., 2006) probe, whose measurement range is 10-1280 μm , and the Two-
629 Dimensional Cloud (2DC; Knollenburg, 1976) probe, whose measurement range is 25-800 μm . OAPs designed for
630 precipitation particle imaging include the Precipitation Imaging Probe (PIP; Baumgardner et al., 2001) and the High
631 Volume Precipitation Spectrometer (HVPS; Lawson et al., 1998), which measure particles ranging from $\sim 100 \mu\text{m}$
632 up to several millimeters.

633 Because an estimate of the sample volume from which a particle is drawn is a function of the particle's size
634 and assumes that the particle is spherical (Brenguier et al., 2013), all PSD probes suffer from sample volume
635 uncertainty. Estimated sample volumes from OAPs perforce suffer from the problem of sizing aspherical particles
636 from 2D images (see Fig 5-40, Brenguier et al., 2013). Nonetheless, impactor and light scattering probes both suffer
637 from much smaller sample volumes than do OAPs (Brenguier et al., 2013; Baumgardner et al., 2017; Heymsfield et
638 al., 2017). Scattering probes, for example, need up to several times the sampling distance in cloud as OAPs to
639 produce a statistically significant PSD estimate (see Fig. 5-3, Brenguier et al, 2013).

640 The obvious difficulty in sizing small ice crystals with light scattering probes is the application of Mie
641 theory to nonspherical ice crystals. Probes such as the FSSP and CDP are therefore prone to undersizing ice crystals

642 [\(Baumgardner et al., 2011; Brenguier et al., 2013; Baumgardner et al., 2017\).](#)

643 [Imaging particles using an OAP requires no assumptions regarding particle shape or composition, but](#)

644 [sizing algorithms based on two-dimensional images are highly sensitive to particle orientation \(Brenguier et al.,](#)

645 [2013\). Other sizing uncertainties stem from imperfect thresholds for significant occultation of photodiodes, the lack](#)

646 [of an effective algorithm for bringing out-of-focus ice particles into focus, and the use of statistical reconstructions](#)

647 [of partially imaged ice crystals that graze a probe's sample area \(Brenguier et al., 2013; Baumgardner et al., 2017\).](#)

648 [Ideally, PSDs estimated using different probes would be stitched together in order to provide a complete](#)

649 [picture of the ice particle population, from micron-sized particles through snowflakes \(Brenguier et al., 2013\).](#)

650 [However, while data from VIPS, fast FSSP, and Small Ice Detector-3 \(SID-3; Ulanowski et al., 2014\) probes are](#)

651 [available to complement the OAP data used in this study, none of them are used on account of sizing uncertainties](#)

652 [stemming from their small sample volumes and from spherical particle assumptions. The two publications](#)

653 [wherewith comparison is made in this paper also restricted their datasets to OAPs.](#)

654 [The main, remaining source of small particle counting and sizing dealt with in this study is particle](#)

655 [shattering. Shattering](#) of ice particles on probe tips and inlets and on aircraft wings has rendered many historical

656 cirrus datasets suspect (Vidaurre and Hallet, 2009; Korolev et al., 2011; [Baumgardner et al., 2017](#)) due to such

657 shattering's artificially inflating measurements of small ice particle concentrations (see, e.g., McFarquhar et al.,

658 2007; Jensen et al., 2009; and Zhao et al., 2011). Measured ice particle size distributions (PSDs) are used to

659 formulate parameterizations of cloud processes in climate and weather models, so the question of the impact of

660 crystal shattering on the historical record of ice PSD measurements is one of significance (Korolev and Field, 2015).

661 Post-processing of optical probe data based on measured particle inter-arrival times (Cooper, 1978; Field et

662 al., 2003; Field et al., 2006; Lawson, 2011; Jackson et al., 2014; Korolev and Field, 2015) has become a tool for

663 ameliorating contamination from shattered artifacts. Shattered particle removal is based on modeling particle inter-

664 arrival times by a Poisson process, assuming that each inter-arrival time is independent of all other inter-arrival

665 times. Jackson and McFarquhar (2014) posit that particle clustering (Hobbs and Rangno, 1985; Kostinski and Shaw,

666 2001; Pinsky and Khain, 2003; Khain et al., 2007), which would violate this basic assumption, is not likely a matter

667 of significant concern as cirrus particles are naturally spread further apart than [are](#) liquid droplets and sediment over

668 a continuum of size-dependent speeds.

669 [In addition, a](#) posteriori shattered particle removal should be augmented with design measures such as

670 specialized probe arms and tips (Vidaurre and Hallet, 2009; Korolev et al., 2011; Korolev et al., 2013a; Korolev and
671 Field, 2015). Probes must also be placed away from leading wing edges (Vidaurre and Hallet, 2009; Jensen et al.,
672 2009), as many small particles generated by shattering on aircraft parts are likely not be filtered out by shatter-
673 recognition algorithms.

674 The ideal way to study the impact of both shattered particle removal and improved probe design is to fly
675 two versions of a probe—one with modified design and one without—side by side and then to compare results from
676 both versions of the probe both with and without shattered particle removal. Results from several flight legs made
677 during three field campaigns where this was done are described in three recent papers: Korolev et al. (2013b),
678 Jackson and McFarquhar (2014), and Jackson et al. (2014). Probes built for several particle size ranges were
679 examined, but those of interest here are the 2D-S and the older 2DC. Three particular results distilled from those
680 papers are useful here.

681 First, [in agreement with Lawson \(2011\)](#), a posteriori shattered particle removal is more effective at
682 reducing counts of apparent shattering fragments for the 2D-S than are modified probe tips. The opposite is true for
683 the 2DC. This is attributed to the 2D-S' larger sample volume, [its](#) improvements in resolution and [electronic time](#)
684 [response over the 2DC](#), [and to its 256 photodiode elements \(Jensen et al., 2009; Lawson, 2011; Brenguier et al.,](#)
685 [2013\)](#), which allow it to size particles smaller than 100 μm and to measure particle inter-arrival times more
686 accurately (Lawson et al., 2010; Korolev et al., 2013b; [Brenguier et al., 2013](#)).

687 Second, shattered artifacts seem mainly to corrupt particle size bins less than about 500 microns ([see also,](#)
688 [Baumgardner et al., 2011](#)). Thus Korolev et al. (2013b) posit that bulk quantities computed from higher order PSD
689 moments, such as shortwave extinction coefficient, IWC, and radar reflectivity, are likely to compare much better
690 between the 2D-S and the 2DC than is N_T ([see also, Jackson and McFarquhar, 2014; Heymsfield et al., 2017](#)).

691 Third, the efficacy of shattered particle removal from the 2DC is questionable: [the](#) post-processing is prone
692 to accepting shattered particles and to rejecting real particles (Korolev and Field, 2015). The parameters of the
693 underlying Poisson model and its ability to correctly identify shattered fragments depend on the physics of the cloud
694 being sampled (Vidaurre and Hallett, 2009; Korolev et al., 2011), [and the older 2DC experiences more issues](#) with
695 instrument depth-of-field, unfocused images, and image digitization [than do newer OAPs](#), further compounding
696 uncertainty [in the shattered particle removal](#) (Korolev et al., 2013b; Korolev and Field, 2015).

697 In the context of relatively small studies such as these, Korolev et al. (2013b) pose two questions: “(i) to

698 what extent can the historical data be used for microphysical characterization of ice clouds, and (ii) can the historical
699 data be reanalyzed to filter out the data affected by shattering?” One difficulty in addressing these questions is the
700 scarcity of data from side-by-side instrument comparisons. Another is that, especially for the 2DC, “correcting
701 [data] a posteriori is not a satisfactory solution” (Vidaurre and Hallet, 2009). However, shattered particle removal is
702 the main (if not the only) correction method available when revisiting historical datasets.

703 In order to address Korolev et al.’s (2013b) first question, bulk cloud properties derived from shatter-
704 corrected 2D-S data are used to answer two questions: 1) How similar are the statistics of cirrus PSD datasets
705 collected using the 2D-S probe to cirrus PSD datasets collected using older 2DC and 2DP probes? 2) How similar
706 are the datasets when shatter-correcting post-processing is applied to the 2DC datasets? In proceeding, two points
707 are critical to recall. First, the 2D-S is reasonably expected to give results superior to the 2DC after shattered
708 particle removal. Second, lingering uncertainty notwithstanding, results presented elsewhere from the shatter-
709 corrected 2D-S reveal behaviors in ice microphysics within different regions of cloud that are expected both from
710 physical reasoning and from modeling studies and that were not always discernible before from in situ datasets
711 (Lawson, 2011; Schwartz et al., 2014).

712 To this end, a substantial climatology of shatter-corrected, 2D-S-measured cirrus PSDs is indirectly
713 compared with two large collections of older datasets, collected from the early 1990s through the mid-2000s mainly
714 using Particle Measurement Systems 2DC and Two-Dimensional Precipitation (2DP) probes (Baumgardner, 1989)
715 as well as Droplet Measurement Technologies Cloud- and Precipitation-Imaging Probes (CIP and PIP; Heymsfield
716 et al., 2009), and in one instance, the 2D-S. The older datasets are presented and parameterized in Delanoë et al.
717 (2005; hereinafter D05) and in Delanoë et al. (2014; hereinafter D14). The data used in D05 were not subject to
718 shattered particle removal, whereas the data in D14 were a posteriori.

719 The comparison strategy, in short is as follows. The D05/D14 parameterizations consist of normalized,
720 “universal” cirrus PSDs to which functions of PSD moments are applied as inputs. The results of so doing are sets
721 of parameterized 2DC PSDs—both shatter-corrected and uncorrected. To make the comparison, the same moments
722 from 2D-S-measured PSDs are applied to the D05/D14 parameterizations in order to simulate what the shatter- and
723 non-shatter-corrected 2DCs would have measured had they flown with the 2D-S. Then, a “universal” PSD derived
724 from the 2D-S itself is computed in order to make a fair comparison. The moments from the 2D-S-measured PSDs
725 are applied to the 2D-S “universal” PSD and it is then seen whether the older datasets differ statistically from the

726 | newer [in their](#) derived cirrus bulk properties. [This procedure is illustrated in Fig. 1.](#)

727 | Section 2 contains a description of the data used herein. Section 3 discusses the fitting of PSDs with
728 | gamma distributions for computational use, Section 4 discusses the normalization and parameterization schemes
729 | used by D05/D14, and Section 5 discusses the effects of not having included precipitation probe data with the 2D-S
730 | data. Section 6 demonstrates the final results of the comparison [and concludes with a discussion.](#)

731 | **2 Data**

732 | The 2D-S data was collected during the Mid-Latitude Airborne Cirrus Experiment (MACPEX), based in
733 | Houston, TX during February and March, 2011 (MACPEX Science Team, 2011); the Small Particles in Cirrus
734 | (SPartICus) campaign, based in Oklahoma during January through June, 2010 (SPartICus Science Team, 2010); and
735 | TC⁴, based in Costa Rica during July, 2007 (TC⁴ Science Team, 2007). The SPEC 2D-S probe (Lawson, 2011)
736 | images ice crystal cross-sections via two orthogonal lasers that illuminate two corresponding linear arrays of 128
737 | photodiodes. PSDs, as well as distributions of cross-sectional area and estimated mass, are reported every second in
738 | 128 size bins with centers starting at 10 microns and extending out to 1280 microns. Particles up to about three
739 | millimeters can be sized in one dimension by recording the maximum size along the direction of flight. During
740 | SPartICus the 2D-S flew aboard the SPEC Inc. Learjet, while during MACPEX it was mounted on the NASA WB57
741 | aircraft. During TC⁴ it was mounted on both the NASA DC8 and the NASA WB57, but the WB57 data is not used
742 | due to documented contamination of the data from shattering artifacts off of the aircraft wing (Jensen et al., 2009).

743 | Temperature was measured during MACPEX, TC⁴, and SPartICus using a Rosemount total temperature
744 | probe. Bulk IWC measurements are available for MACPEX from the Closed-path tunable diode Laser Hygrometer
745 | (CLH) probe (Davis et al., 2007). Condensed water that enters the CLH is evaporated so that a measurement of total
746 | water can be made. The condensed part of the total water measured by the CLH is obtained by estimating
747 | condensed water mass from concurrent PSDs measured by the National Center for Atmospheric Research (NCAR)
748 | Video Image Particle Sampler (VIPS) probe and then subtracting this estimate from the measured total water mass.

749 | **3 Parametric Fitting of PSDs**

750 | PSDs measured by the 2D-S were fit with both unimodal and bimodal parametric gamma distributions.

751 | The unimodal distribution is

752 |
$$n(D) = N_0 \left(\frac{D}{D_0} \right)^\alpha \exp\left(-\frac{D}{D_0} \right), \quad (1)$$

753 where D is particle maximum dimension, D_0 is the scale parameter, α is the shape parameter, and N_0 is the so-called
754 intercept parameter. The bimodal distribution is simply a mixture of two unimodal distributions:

$$755 \quad n(D) = N_{01} \left(\frac{D}{D_{01}} \right)^{\alpha_1} \exp\left(-\frac{D}{D_{01}}\right) + N_{02} \left(\frac{D}{D_{02}} \right)^{\alpha_2} \exp\left(-\frac{D}{D_{02}}\right). \quad (2)$$

756 Save in a handful of instances (which will be indicated), all bulk PSD quantities shown here are computed using
757 these parametric fits. A combination of unimodal and bimodal fits is used to compute N_T , dictated by the shape of
758 the PSD as determined by a generalized chi-squared goodness of fit test (Schwartz., 2014). Unimodal fits are used
759 to compute all other bulk quantities.

760 Unimodal fits were performed via the method of moments [in a manner similar to Heymsfield et al.
761 (2002)]. Both the method of moments and an expectation maximization algorithm (Moon, 1996; Schwartz, 2104)
762 were used for the bimodal fits; the more accurate of those two fits [as determined by whether fit provided the
763 smaller binned Anderson-Darling test statistic (Demortier, 1995)] being kept.

764 Measured PSDs are both truncated and time-averaged in order to mitigate counting uncertainties. It is here
765 assumed that temporal averaging sufficiently reduces Poisson counting noise so that it may be ignored [see, e.g.,
766 Gayet et al. (2002)]. Given already cited concerns regarding uncertainty in shattered particle removal, the smallest
767 size bins are not automatically assumed here to be reliable. Other competing uncertainties further complicate
768 particle counts within the first few size bins, e.g., [decreased detection efficiency within the first size bin](#)
769 [\(Baumgardner et al., 2017\)](#), the possible underestimation of counts of real particles by a factor of 5-10 (Gurganus
770 and Lawson, 2016), and mis-sizing of larger [particles](#) into smaller size bins due to image break-up at the edge of the
771 instrument's depth of field (Korolev et al., 2013b; Korolev and Field, 2015; [Baumgardner et al., 2017](#)).

772 In order to determine how many of the smallest size bins to truncate and for how many seconds to average
773 in order to make the counting assumption valid, two simple exercises were performed using the MACPEX dataset.
774 In the first exercise, fifteen-second temporal averages were performed along with truncating zero through two of the
775 smallest size bins while only the unimodal fits (chosen according to a maximum likelihood ratio test [Wilks, 2006])
776 were kept. [This exercise was performed first so as to prevent the most spurious size bins' interfering with the](#)
777 [smoothing out of Poisson counting noise](#). Figure 2 shows comparisons of distributions of measured and computed
778 (from the fits) N_T s. The difference in the number of samples of computed N_T between zero bins and one bin
779 truncated is an order of magnitude higher than that between one bin and two bins truncated. This is due to frequent,

780 extraordinarily high numbers of particles recorded in the smallest size bin that at times cause a PSD to be flagged as
781 bimodal by the maximum likelihood ratio test. As this effect lessens greatly after truncating only one bin, and as the
782 computed and measured N_{TS} are otherwise better matched using a single-bin truncation, the smallest size bin is
783 ignored for all PSDs (making the smallest size bin used 15-25 microns).

784 Also, IWC was estimated from the fit distributions (the first size bin having been left off in the fits) using
785 the mass-dimensional relationship $m(D) = 0.0065D^{2.25}$ (m denotes mass, and all units are cgs) given in
786 Heymsfield (2003) for mid-latitude cirrus. The distribution of IWC thus computed nominally matches (not shown)
787 IWC estimates from both the CLH and from the 2D-S data product, which uses mass-projected area relationships
788 (Baker and Lawson, 2006).

789 For the second exercise, temporal averages from one to 20 seconds were performed, truncating the first size
790 bin and again keeping only the unimodal fits. The balance to strike in picking a temporal average length is to
791 smooth out Poisson counting uncertainties acceptably without losing physical information to an overlong average.
792 Qualitatively, the statistics of the fit parameters begin to steady at around 15 seconds (not shown), so a fifteen-
793 second temporal average was chosen. Using the data filters, temporal average, and bin truncation thus far described
794 results in ~17 000 measured PSDs and their accompanying fits.

795 It must be noted that the first 2D-S size bin contains at least some real particles, though the afore-
796 mentioned uncertainties make it impossible (at present) to know how many. Therefore, N_{TS} computed from the
797 remaining bins can be underestimates. Parametric fits extrapolate the binned data all the way to size zero, though;
798 so it could be assumed, if the real ice particle populations are in fact gamma-distributed, that this extrapolation is a
799 fair estimate of the real particles lost due to truncating the first size bin. In truth, however, the assumption of a
800 gamma-shaped PSD is arbitrary, if convenient; but the gamma PSD shape is kept for its convenience and for its
801 ability to reproduce higher-order PSD moments. However, in this paper, where N_{TS} (equivalently, the zeroth
802 moments) from either the parametric, the binned, or the normalized parametric PSDs are computed, the
803 computations are begun at the left edge of the second size bin so as to compare equivalent quantities. In other
804 words, N_{TS} presented for comparison here are truncated to compensate for having left off the smallest size bin.

805 **4 Normalization and Parameterization**

806 In this section, the functions of 2D-S-measured PSD moments that are applied to the D05/D14
807 parameterizations (see Figure 1) are explained. However, the D05 and D14 parameterizations make use of PSDs in

808 terms of equivalent melted diameter D_{eq} . Before computing any moments, it is therefore necessary first to transform
 809 all 2D-S-measured PSDs from functions of maximum dimension D to functions of equivalent melted diameter D_{eq} .

810 Each 2D-S-measured PSD $n_D(D)$, whose independent variable is ice particle maximum dimension, is
 811 transformed to a distribution $n_{D_{eq}}(D_{eq})$ whose independent variable is equivalent melted diameter. The
 812 transformations are performed twice: once using the density-dimensional relationship used in D05 and once using a
 813 mass-dimensional relationship used in D14. The first transformation allows for application of the 2D-S data to the
 814 D05 parameterization, and the second first transformation allows for application of the 2D-S data to the D14
 815 parameterization.

816 The density-dimensional relationship $\rho(D) = aD^b$ (ρ denotes density, D denotes particle maximum
 817 dimension, the power law coefficients are $a = 0.0056$ and $b = -1.1$, and all units are cgs) used in D05 stems
 818 from relationships published by Locatelli and Hobbs (1974) and Brown and Francis (1995) for aggregate particles.
 819 Setting masses equal as in D05 results in the independent variable transformation

$$820 \quad \underline{D_{eq} = \left(\frac{aD^b}{\rho_w} \right)^{1/3} D, \quad (3)}$$

821 where ρ_w is the density of water.

822 The mass-dimensional relationship labeled “Composite” (Heymsfield et al., 2010) in D14 is used here for
 823 the second transformation:

$$824 \quad \underline{m(D) = 7e^{-3}D^{2.2} = a_m D^{b_m} .}$$

825 (Here, m denotes mass, the power law coefficients are $a_m = 7e^{-3}$ and $b_m = 2.2$, and all units are cgs.) Setting
 826 masses equal results in the independent variable transformation

$$827 \quad \underline{D_{eq} = \left(\frac{6a_m}{\pi\rho_w} \right)^{1/3} D^{b_m/3} . \quad (4)}$$

828 The “Composite” relation was only used to normalize about 54% of the PSDs utilized in D14; however, those

829 datasets so normalized are broadly similar to MACPex, SPARTICUS, and TC⁴ (one in fact is TC⁴, where the Cloud
 830 Imaging Probe was used as well as the 2D-S), and so the “Composite” relation is used here for comparison with
 831 D14.

832 Following D05/D14s’ notation, transformed PSDs then have their independent variable scaled by mass-
 833 mean diameter

$$834 \quad D_m = \frac{\int_0^\infty D_{eq}^4 n_{D_{eq}}(D_{eq}) dD_{eq}}{\int_0^\infty D_{eq}^3 n_{D_{eq}}(D_{eq}) dD_{eq}} \quad (5)$$

835 and their ordinates scaled by

$$836 \quad N_0^* = \frac{4^4 \left[\int_0^\infty D_{eq}^3 n_{D_{eq}}(D_{eq}) dD_{eq} \right]^5}{\Gamma(4) \left[\int_0^\infty D_{eq}^4 n_{D_{eq}}(D_{eq}) dD_{eq} \right]^4}, \quad (6)$$

837 so that

$$838 \quad n_{D_{eq}}(D_{eq}) = N_0^* F\left(x = \frac{D_{eq}}{D_m}\right). \quad (7)$$

839 In Eq. (7), $F(x)$ is, ideally, the universal, normalized PSD (Meakin, 1992; Westbrook et al., 2004a,b; D05; Tinel

840 et al, 2005; D14). The quantities N_0^* and D_m are the functions of 2D-S-measured PSD moments that are required

841 for application to the D05/D14 parameterizations in order to produce parameterized, corrected and uncorrected 2DC

842 PSDs (see Figure 1). The procedure for transforming and normalizing the 2D-S-measured PSDs and for computing

843 N_0^* and D_m is now explained.

844 Starting with binned PSDs, the normalization procedure is wended as described in section 4.1 of D05.

845 First, the 2D-S bin centers and bin widths are transformed once using Eq. (3) for the comparison with D05 and once

846 again using Eq. (4) for the comparison with D14. Next, each binned PSD is transformed by scaling from D -space to

847 D_e -space (see below). Then, via numerically computed moments, Eqs. (5)-(7) are used to produce one N_0^* , D_m

848 pair for each measured PSD and to normalize the binned, mass-equivalent spherical PSDs, which are then grouped

849 into normalized diameter bins of $\Delta x = 0.10$.

850 The scale factor for **transforming binned PSDs** is derived **using** this simple consideration: if the number of
851 particles within a size bin is conserved upon the bin's transformation from D -space to D_e -space, then, given that the
852 transformation is from maximum dimension to mass-equivalent spheres, so also is the mass of the particles within a
853 size bin conserved. That is,

$$854 \quad n_{D_{eq}}(D_{eq_i}) = n_D(D_i) \frac{a D_i^{b+3} \Delta D_i}{\rho_w D_{eq_i}^3 \Delta D_{eq_i}} \quad (8)$$

855 for the D05 transformation and

$$856 \quad n_{D_{eq}}(D_{eq_i}) = n_D(D_i) \frac{a_m D_i^{b_m} \Delta D_i}{\left(\frac{\pi}{6}\right) \rho_w D_{eq_i}^3 \Delta D_{eq_i}} \quad (9)$$

857 for the D14 transformation. **(The subscript i is iterated through each size bin.)**

858 Mass-equivalent transformations theoretically ensure that both N_T and IWC can be obtained by using the
859 PSD in either form:

$$860 \quad N_T = \int_0^\infty n_D(D) dD = \int_0^\infty n_{D_{eq}}(D_{eq}) dD_{eq} \quad (10)$$

$$861 \quad IWC = \frac{\pi}{6} \int_0^\infty a D^{b+3} n_D(D) dD = \frac{\pi}{6} \int_0^\infty \rho_w D_{eq}^3 n_{D_{eq}}(D_{eq}) dD_{eq} \quad (11a), \text{ or}$$

$$862 \quad IWC = \int_0^\infty a_m D^{b_m} n_D(D) dD = \frac{\pi}{6} \int_0^\infty \rho_w D_{eq}^3 n_{D_{eq}}(D_{eq}) dD_{eq} \quad (11b)$$

866 **(Whether Eq. (11a) or Eq. (11b) is used depends upon whether the D05 or the D14 transformation is being**
867 **considered.)** As it turns out, scaling from D -space to D_{eq} -space so that Eqs. (10) and (11) are both satisfied is not
868 necessarily possible. Since for the sake of estimating $\underline{D_m}$ and $\underline{N_0^*}$ it is more important that IWCs be matched, this
869 was done for the D05 comparison while matching the N_T s to within a factor of approximately 0.75, plus a bias of
870 $\sim 3.1 \text{ L}^{-1}$.

871 The following transformation of variables must be used for computing other bulk quantities from

872 transformed PSDs (Bain and Englehardt, 1992):

873
$$n_D(D) = n_{D_{eq}} \left[D_{eq}(D) \right] \left| \frac{dD_{eq}}{dD} \right|^{-1}. \quad (12)$$

874 For instance, effective radar reflectivity is computed [by integrating over particle maximum dimension intervals](#),
875 using a set of [particle maximum dimension/backscatter power-laws that were fit piecewise from](#) T-matrix
876 computations of backscatter cross section to particle maximum dimension (Matrosov, 2007; Matrosov et al., 2012;
877 Posselt and Mace, 2013; Hammonds et al., 2014) as follows:

878
$$Z_e = \frac{10^8 \lambda^4}{|K_w|^2 \pi^5} \sum_j \int_{D_j}^{D_{j+1}} a_{zj} D^{b_{zj}} n_{D_{eq}} \left[D_{eq}(D) \right] \left| \frac{dD_{eq}}{dD} \right| dD$$

879 The [set of power law](#) coefficients (a_{zj}, b_{zj}) [was](#) derived assuming an air/ice dielectric mixing model and that all
880 particles are prolate spheroids with aspect ratios of 0.7 (Korolev and Isaac, 2003; Westbrook et al., 2004a;
881 Westbrook et al., 2004b; Hogan et al., 2012). Several explicit expressions for computing bulk quantities based on
882 equivalent distributions may be found in Schwartz (2014).

883 In D05/D14, data taken with cloud particle and precipitation probes were combined to give PSDs ranging
884 from 25 μm to several millimeters. No precipitation probe data is used here, but how does not including
885 precipitation probe data affect the comparison? This question will be addressed later in this paper.

886 Two-dimensional histograms of the normalized PSDs are shown in Fig. [3](#) for the D05 transformation and in
887 Fig. [5](#) for the D14 transformation, overlaid with their mean normalized PSDs (cf. Figs. 1 and 2 in D05 and Fig. 3 in
888 D14). For both transformations, the mean normalized PSDs for the three datasets combined are repeated in Figs. [4](#)
889 and [6](#) as solid curves (cf. Fig. 3 of D05 and Fig. 6 of D14). These serve as the empirical universal, normalized PSDs

890 $F_{\sim 2DS-D05}(x)$ and $F_{\sim 2DS-D14}(x)$, derived using the mass transformations of D05 and D14, respectively. They,
891 and the quantities derived therefrom, serve to [parameterize](#) the more modern 2D-S with shattered particle removal.
892 The subscripts $\sim 2DS-D05$ and $\sim 2DS-D14$ are used hereinafter to represent bulk quantities derived using

893 $F_{\sim 2DS-D05}(x)$ and $F_{\sim 2DS-D14}(x)$.

894 Three parametric functions for $F(x)$ are given in D05, two of which are repeated here: the gamma- μ

895 function (F_μ) and the modified gamma function ($F_{\alpha,\beta}$; Petty and Huang, 2011).

896
$$F_\mu(x) = \frac{\Gamma(4)(4+\mu)^{4+\mu}}{4 \Gamma(4+\mu)} x^\mu \exp[-(4+\mu)x] \quad (13)$$

897
$$F_{\alpha,\beta}(x) = \beta \frac{\Gamma(4) \Gamma\left(\frac{\alpha+5}{\beta}\right)^{4+\alpha}}{4^4 \Gamma\left(\frac{\alpha+4}{\beta}\right)^{5+\alpha}} x^\alpha \exp\left[-\left(\frac{\Gamma\left(\frac{\alpha+5}{\beta}\right)}{\Gamma\left(\frac{\alpha+4}{\beta}\right)}\right)^\beta\right] \quad (14)$$

898 Values of μ , α , and β can be chosen to fit these functions to a mean normalized PSD. In D05, the parametric
 899 functions $F_{\alpha,\beta} = F_{(-1,3)}$ (Eq. (14)) and $F_\mu = F_3$ (Eq. (13)) are given to approximate the universal PSD derived
 900 from combined 2DC-2DP datasets; and in D14, the parametric function $F_{\alpha,\beta} = F_{(-0.262,1.754)}$ is given to
 901 approximate the universal PSD derived from shatter-corrected datasets collected mainly with combined 2DC-2DP
 902 probes.

903 These functions are used to parameterize transformed PSDs measured by the 2DC-2DP, given N_0^* and
 904 D_m . We therefore make the assumption that if we take N_0^* and D_m derived from a 2D-S-measured PSD and then
 905 apply them to Eq. (13) or (14), we have effectively simulated the parameterized, transformed PSD that a combined
 906 2DC-2DP would have observed had they been present with the 2D-S. The subscripts $\sim 2DCu$ and $\sim 2DCs$ are used
 907 hereinafter to represent quantities that simulate 2DC-2DP data (non-shatter-corrected and shatter-corrected,
 908 respectively) in this way. Thus, we begin with two versions of $F_{\sim 2DCu}(x) = F_\mu = F_3$ and $F_{\alpha,\beta} = F_{-1,3}$ —and
 909 one version of $F_{\sim 2DCs}(x) = F_{\alpha,\beta} = F_{(-0.262,1.754)}$ —Initial observations on comparison of $F_{\sim 2DS-D05}(x)$ and
 910 $F_{\sim 2DS-D14}(x)$ with $F_{\sim 2DCu}(x)$ and $F_{\sim 2DCs}(x)$ will now be given.

911 4.1 Comparison with D05

912 Some important qualitative observations can be made from examining $F_{\sim 2DS-D05}(x)$ in Fig. 4. First, in
 913 contrast to Fig. 3 of D05, the concentrations of particles at the smallest scaled diameters of $F_{\sim 2DS-D05}(x)$ are, on

914 | average, about an order of magnitude or more lower [than for the mean, normalized PSD in D05](#). From this it is
 915 | surmised that while the 2D-S continues to register relatively high numbers of small ice particles, the number has
 916 | decreased in the newer datasets due to the exclusion of [larger numbers of](#) shattered ice crystals.

917 | It can also be seen in Fig. 4 that the shoulder in the normalized PSDs in the vicinity of $x \sim 1.0$ exists in the
 918 | newer data as it does in the data used in D05. It is worth noting, though, that the shoulder exists in the one tropical
 919 | dataset used here (TC⁴), whereas it is absent or much less noticeable in the tropical datasets used in D05.

920 | Fortuitously, $F_{\alpha,\beta} = F_{(-1,3)}$ fits the 2D-S data better than it does the older data [in D05](#) at the smallest
 921 | normalized sizes (cf. Fig. 2 in D05). Neither $F_{\alpha,\beta} = F_{(-1,3)}$ nor $F_{\mu} = F_3$ correctly catches the shoulder in the
 922 | newer data, though $F_{\alpha,\beta} = F_{(-1,3)}$ was formulated to (better) catch a corresponding shoulder in the older data.

923 | Next, a comparison of PSD quantities computed directly from the 2D-S with corresponding $\sim 2DC$ -derived
 924 | quantities (computed using N_0^* and D_m derived directly from the binned 2D-S data and applied to $F_{\alpha,\beta} = F_{(-1,3)}$
 925 | and $F_{\mu} = F_3$) is made. The extinction coefficient, IWC, and 94 GHz radar reflectivity compare well between the
 926 | 2D-S and both versions of $\sim 2DCu$ (not shown). As for N_T , it is the least certain computation (see Fig. 7); but
 927 | $F_{\mu} = F_3$ is entirely wrong in attempting to reproduce this quantity, so this shape is not used hereinafter and
 928 | $F_{\sim 2DCu}(x) = F_{(-1,3)}(x)$ is the shape used to simulate the uncorrected 2DC-2DP.

929 | Figure 8 shows the mean relative error and the standard deviation of the relative error (cf. Fig. 5 of D05)
 930 | between 2D-S-derived and corresponding $\sim 2DCu$ -derived quantities. Effective radius is as defined in D05. Mean
 931 | relative error for both extinction coefficient and IWC is about -0.1%. The mean relative error in N_T (N_T computed
 932 | directly from [truncated](#), binned PSDs is used both here and in Fig. 9) is rather large at $\sim 50\%$; and the mean relative
 933 | error in Z_e , at $\sim 22\%$, is larger than that shown in Fig. 5 of D05 (less than 5% there) but, at about 2 dB, is within the
 934 | error of most radars. This may well be due to the overestimation of $F(x)$ by $F_{\sim 2DCu}(x)$ between normalized
 935 | sizes of about 1.2 and 2 [see Fig. 4b]. Both here and in D05, $F_{\sim 2DCu}(x)$ falls off much more rapidly than
 936 | $F_{\sim 2DS-D05}(x)$ above a normalized diameter of two. However, it is deduced from Figs. 2 and 5 in D05 that this

937 roll-off is not responsible for the large mean relative error in Z shown in Fig. 8.

938 The mean relative error in effective radius shown in Fig. 8 is approximately -7%, whereas it is apparently
939 nil in Fig. 5 of D05. Effective radius is defined in D05 as the ratio of the third to the second moments of the
940 spherical-equivalent PSDs and is therefore a weighted mean of the PSD. The negative sign on the relative error
941 indicates that, on average, $F_{\sim 2DCu}(x)$ is underestimating the effective radius of the PSDs measured by the 2D-S
942 whereas for the older datasets it hits the effective radius spot-on (in the average). Therefore, there is a significant
943 difference between the 2D-S datasets and the older 2DC-2DP datasets in the ratio of large particles to small
944 particles, even when precipitation probe data is not combined with the 2D-S.

945 4.2 Comparison with D14

946 From Fig. 5, concentrations at the smallest scaled diameters of $F_{\sim 2DS-D14}(x)$ are nominally consistent
947 with those shown in Fig. 6 of D14. In accordance with the surmise made in the comparison with D05 above, it
948 would seem that shattered particle removal from the 2DC improves comparison between the 2D-S and the 2DC-2DP
949 at the smallest particle sizes.

950 Here, $F_{\sim 2DCs}(x) = F_{(-0.262, 1.754)}(x)$. The shoulder in the normalized PSDs in the vicinity of $x \sim 1.0$ is
951 again found, though the shoulder is not captured by $F_{\sim 2DCs}(x)$ (see Fig. 6). The normalized 2D-S at the smallest
952 normalized sizes is also underestimated by $F_{\sim 2DCs}(x)$. Comparison of N_T computed using $F_{\sim 2DCs}(x)$ with that
953 derived from 2D-S is quite similar to that of $F_{\sim 2DCu}(x)$ (not shown).

954 As shown in Fig. 9, the mean relative error between N_T and effective radius derived from the 2D-S and
955 from $\sim 2DCs$ is again about 50%, while the mean relative error in effective radius remains about -7.5%. The mean
956 relative error in reflectivity has decreased to about 14%.

957 5 Impact of Not Using Precipitation Probe Data

958 To more formally investigate the impact of not using a precipitation probe, data from the PIP were
959 combined with data from the 2D-S using the TC⁴ dataset. This campaign of the three was chosen due to its tending
960 to occur at warmer temperatures, in a more convective environment, and at lower relative humidities: therefore, if
961 large particles are going to matter, they should matter for TC⁴. Figure 10 shows, similar to Figs. 4 and 6,

962 $F_{\sim 2DS-D05}(x)$ for the 2D-S alone, $F_{\sim 2DS/PIP-D05}(x)$ for the 2D-S combined with the PIP, and $F_{\sim 2DCu}(x)$.

963 In the combined data, $F_{\sim 2DS/PIP-D05}(x)$ does not dig as low between zero and unity as for the 2D-S alone;

964 but it does show similar numbers of particles at the very smallest normalized sizes, and the shoulder is in the same
965 location. Beginning at about $x = 1.2$, the 2D-S-PIP normalized distribution is higher than the 2D-S-alone

966 normalized distribution; and it continues out to about $x = 10$, whereas the 2D-S-alone distribution ends shy of $x = 5$.

967 In either case, $F_{\sim 2DCu}(x)$ misses what is greater than about $x = 2$. This roll-off, along with the fact that

968 $F_{\sim 2DS/PIP-D05}(x)$ appears to be more similar to $F_{\sim 2DS-D05}(x)$ than it does to $F_{\sim 2DCu}(x)$, indicate that a

969 parameterization of $F(x)$ based off the 2D-S alone is comparable to the 2DC/2DP-based $F_{\sim 2DCu}(x)$

970 parameterization.

971 In support of this assertion, Fig. 11 shows the penalty in radar reflectivity, computed directly from data

972 using the approach described earlier, incurred by using only the 2D-S instead of the 2D-S-PIP. The penalty is in the

973 neighborhood of 1 dB.

974 The true ([in the sense that they are derived directly from measurements](#)) N_0^* and D_m computed from each

975 of the 2D-S PSDs alone and from the combined PSDs from TC⁴ were used, along with $F_{\sim 2DCu}(x)$, to compute N_T ,

976 extinction coefficient, IWC, and 94 GHz effective radar reflectivity. This amounts to two different $\sim 2DCu$

977 simulations: one including the PIP and one not. The results are shown in Fig. 12. The distributions are very

978 similar, with the exception of the reflectivity distributions, whose means are separated by less than 1 dBZ. It is

979 concluded that the cloud filtering technique has resulted in PSDs that are satisfactorily described by the 2D-S alone,

980 at least in the case of this comparison.

981 6 Final Results and Discussion

982 In D05, complete parameterization of a 2DC-2DP-measured PSD is achieved by using [the](#) universal shape

983 $F_{\alpha,\beta}(x)$ along with N_0^* parameterized by radar reflectivity and D_m parameterized by temperature. For

984 comparison with the shattered-corrected D14 study, a temperature-based parameterization of “composite”-derived

985 D_m is also [computed](#) from the 2D-S data and “composite”-derived N_0^* is [also](#) parameterized by radar reflectivity.

986 A similar parameterization scheme (also based on radar reflectivity and temperature) for the 2D-S (based on Field et
987 al., 2005) is outlined in Schwartz (2014) and is used here to compute a fully parameterized version of 2D-S-
988 measured PSDs so as to make a fair comparison of them with fully parameterized 2DC-2DP-measured PSDs.

989 Figure 13 shows the results of computing PSD-based quantities using the fully parameterized 2D-S (red,
990 labeled “ $x2DS$ ”), the fully parameterized (uncorrected) 2DC-2DP (blue, labeled “ $x2DCu$ ”), and directly from the
991 2D-S data (black). Probability density functions (pdfs) of 94 GHz effective radar reflectivity match because they
992 are forced to by the two instrument parameterizations. Otherwise, biases exist between the two sets of computations
993 based on simulated instruments and computations based on the actual 2D-S (black curve). This bias is due mainly to
994 the temperature parameterization of D_m . The pdfs of extinction coefficient and IWC for the two parameterized
995 instruments match one another quite well (the differences in their medians are not statistically significant).
996 However, for N_T , the $x2DCu$ pdf is shifted to higher concentrations than the pdf for $x2DS$. The difference in their
997 medians is statistically significant at the 95% level according to a Mann-Whitney U test. It is therefore concluded
998 that the older D05 parameterization based on the 2DC-2DP data sets predicts a statistically significant higher
999 number of total ice crystals than does the parameterized 2D-S (by a factor of about 1.3, or a little over 1 dB) and
1000 that, more generally, the 2DC measures a larger ratio of small ice crystals to large ice crystals than does the 2D-S, as
1001 shown in the effective radius comparison in Fig. 8.

1002 Figure 14 shows pdfs of N_T and extinction coefficient computed using the fully parameterized 2D-S (red,
1003 labeled “ $x2DS$ ”), the fully parameterized (corrected) 2DC-2DP (blue, labeled “ $x2DCs$ ”), and directly from the 2D-S
1004 data (black). The pdfs of extinction match quite well, but their medians are significantly different according to the U
1005 test. The medians of N_T are also significantly different, but the mean of the parameterized, corrected 2DC is lower
1006 than that of the parameterized 2D-S. A posteriori shatter correction has made 2DC measurements more like 2D-S
1007 measurements in the bulk quantity of total particle concentration, however, a statistically significant difference
1008 between the 2D-S and the corrected 2DC remains. This result is entirely expected in light of the previous results
1009 outlined in the introduction to this paper.

1010 In this paper, an indirect comparison to older, 2DC-based datasets by means of parameterizations given in
1011 D05 and in D14 has been made. The main discussion points and some sources of uncertainty are now enumerated.

1012 2) It is determined that the 2D-S cirrus cloud datasets used here are significantly different from historical
1013 datasets in numbers of small ice crystals measured. With a posteriori shattered particle removal applied to

1014 older 2DC data, the total numbers of ice crystals measured by the 2D-S and the 2DC become more similar,
1015 but NT measured by the 2DC remains statistically different from that measured by the 2D-S.

1016 3) Given the modest differences found here between bulk cirrus properties derived from PSDs, we conclude
1017 that historical data sets continue to be useful. It would seem that for the measurement of bulk cirrus
1018 properties—excepting N_T —instrument improvements may have produced only marginal improvements.

1019 4) It is surmised that, since the efficacy of a posteriori shatter correction on the 2DC is questionable and since
1020 the 2D-S is superior in response time, resolution, and sample volume to the 2DC, and since steps were
1021 taken to mitigate ice particle shattering on the 2D-S data, that the newer data sets are more accurate.
1022 Therefore, continuing large-scale field investigations of cirrus clouds using newer particle probes and data
1023 processing techniques is recommended. Where possible, investigation of the possibility of statistical
1024 comparison and correction of historical cirrus ice particle datasets using newer datasets by flying 2DC
1025 probes alongside 2D-S and other, more advanced probes is strongly encouraged.

1026 5) There are some sources of uncertainty.

1027 a. There exists a large amount of uncertainty in mass- and density-dimensional relationships for ice
1028 crystals, such as those used in D05, D14, and in this paper. In making a comparison, the best that
1029 could be done was to use the same relations in this paper as in D05 and D14. This, of course—
1030 depending on which part of the comparison is considered—assumes either that the same overall
1031 mix of particles habits was encountered between D05 and this study and between D14 and this
1032 study.

1033 b. The data for both D05 and D14 is stated to begin at 25 μm , whereas the 2D-S data used here is
1034 truncated to begin at 15 μm . This means that the 2D-S data had the potential of measuring greater
1035 numbers of small particles than did the 2DC, and yet the differences in small particles between
1036 D05 and the current study were still realized.

1037 6) Finally, it is important to note that this study does not specifically consider PSD shape. [\(For a more](#)
1038 [detailed discussion on cirrus PSD shape and on the efficacy of the gamma distribution, please refer to](#)
1039 [Schwartz \[2014\].\)](#) This is a critical component of the answers to Korolov et al.'s (2013b) original two
1040 questions. Mitchell et al. (2011) demonstrated that for a given effective diameter and IWC, the optical
1041 properties of a PSD are sensitive to its shape. Therefore, PSD bimodality and concentrations of small ice

1042 crystals are critical to realistically parameterizing, cirrus PSDs, to modeling their radiative properties and
1043 sedimentation velocities, and to mathematical forward models designed to infer cirrus PSDs from remote
1044 sensing observations (Lawson et al., 2010; Mitchell et al, 2011; Lawson, 2011). In order to improve
1045 knowledge on PSD shape, as well as to develop statistical algorithms for correcting historical PSD datasets
1046 so that PSD shapes are corrected along with computations of bulk properties, it will be necessary to make
1047 use of instruments that can provide reliable measurements of small ice crystals beneath the size floors of
1048 both the 2DC and the 2D-S. Recent studies such as Gerber and DeMott (2014) have provided aspherical
1049 correction factors for particle volumes and effective diameters measured by the FSSP. However, the author
1050 expects that this problem will ultimately be resolved by the continued technological development of new
1051 probes such as the HOLODEC.

1052 **Data Availability**

1053 All SPartICus data may be accessed via the Atmospheric Radiation Measurement (ARM) data archive as
1054 noted in the references. All MACPEX and TC⁴ data may be accessed from the NASA Earth Science Project Office
1055 (ESPO) data archive, also noted in the references.

1056 **ACKNOWLEDGEMENTS**

1057 The author gratefully acknowledges the SPartICus, MACPEX, and TC⁴ science teams for the collection of
1058 data used in this study. TC⁴ and MACPEX data were obtained from the NASA ESPO archive, which may be
1059 accessed online at <https://espoarchive.nasa.gov/archive/browse/>. The SPartICus data were obtained from DOE
1060 ARM archive and may be accessed online at
1061 <http://www.archive.arm.gov/discovery/#v/results/s/fiop::aaf2009Sparticus>. In particular, the author acknowledges
1062 Dr. Paul Lawson and SPEC, Inc. for all 2D-S data collected in the field, to Dr. Andrew Heymsfield for the PIP data
1063 used from TC⁴, and to Dr. Linnea Avallone for CLH data used from MACPEX. Thanks are furthermore given to
1064 Drs. Gerald G. Mace, Paul Lawson, and Andrew Heymsfield for helpful discussions that led to significant
1065 improvements in the manuscript. This work was supported by the U.S. Department of Energy's (DOE) Atmospheric
1066 System Research (ASR), an Office of Science, Office of Biological and Environmental Research (BER) program,
1067 under Contract DE-AC02-06CH11357 awarded to Argonne National Laboratory. This work was also supported by
1068 the National Science Foundation (NSF) Grant AGS-1445831. Grateful acknowledgement is also given to the
1069 computing resources provided on Blues, a high-performance computing cluster operated by the

1070 Laboratory Computing Resource Center (LCRC) at the Argonne National Laboratory.

1071 **Competing Interests**

1072 The author declares that he has no conflict of interest.

1073 **REFERENCES**

- 1074 Bain, L. J. and M. Englehardt, 1992: *Introduction to Probability and Mathematical Statistics*,
 1075 *2nd Ed.* Duxbury Press, 644 pp.
 1076
- 1077 Baker, B. A. and R. P. Lawson, 2006: Improvement in determination of ice water content from
 1078 two-dimensional particle imagery. Part I: Image-to-mass relationships. *J. Appl. Meteor. Climatol.*, **45**,
 1079 1282-1290.
 1080
- 1081 Baumgardner, D., 1989: Airborne Measurements for Cloud Microphysics. *Res. Aviat. Facility*
 1082 *Bull.*, **24**, 1-22.
 1083
- 1084 [Baumgardner, D., H. Jonsson, W. Dawson, D. O'Connor, and R. Newton, 2001: The cloud, aerosol and](#)
 1085 [precipitation spectrometer \(CAPS\): A new instrument for cloud investigations. *Atmos. Res.*, **59-60**, 251-](#)
 1086 [264, doi:10.1016/S0169-8095\(01\)00119-3.](#)
 1087
- 1088 [Baumgardner, D., and Coauthors, 2011: Airborne instruments to measure atmospheric aerosol particles, clouds and](#)
 1089 [radiation: A cook's tour of mature and emerging technology. *Atmos. Res.*, **101**, 10-29,](#)
 1090 [doi:10.1016/j.atmosres.2011.06.021.](#)
 1091
- 1092 [Baumgardner, D. and Coauthors, 2017: In situ measurement challenges. *Ice Formation and Evolution in Clouds*](#)
 1093 [and *Precipitation: Measurement and Modeling Challenges*, Meteor. Monogr., No. 58, Amer. Meteor. Soc.,](#)
 1094 [doi:10.1175/AMSMONOGRAPHIS-D-16-0011.1.](#)
 1095
- 1096 [Brennguier, J.-L., Bachalo, W. D., Chuang, P. Y., Esposito, B. M., Fugal, J., Garrett, T., Gayet, J.-F., Gerber, H.,](#)
 1097 [Heymsfield, A., Kokhanovsky, A., Korolev, A., Lawson, R. P., Rogers, D. C., Shaw, R. A., Strapp, W. and](#)
 1098 [Wendisch, M. \(2013\) *In Situ Measurements of Cloud and Precipitation Particles, in Airborne*](#)
 1099 [Measurements for Environmental Research: Methods and Instruments \(eds M. Wendisch and J.-L.](#)
 1100 [Brennguier\), Wiley-VCH Verlag GmbH & Co. KGaA, Weinheim, Germany.](#)
 1101 [doi: 10.1002/9783527653218.ch5](#)
 1102
- 1103 Brown, P. R. A., and P. N. Francis, 1995: Improved Measurements of the Ice Water Content in
 1104 Cirrus Using a Total Water Probe. *J. Atmos. Oceanic Technol.*, **12**, 410-414.
 1105
- 1106 Cooper, W. A., 1978: Cloud physics investigations by the University of Wyoming in HIPLEX
 1107 1977. Department of Atmospheric Science, University of Wyoming, Rep. AS119, 320 pp.
 1108
- 1109 Davis, S. M., A. G. Hallar, L. M. Avallone, and W. Engblom, 2007: Measurements of Ice Water
 1110 Content With a Tunable Diode Laser Hygrometer: Calibration Procedure and Inlet Analysis. *J. Atmos.*
 1111 *Oceanic Technol.*, **24**, 463, doi:10.1175/JTECH1975.1.
 1112
- 1113 Delanoë, J., A. Protat, J. Testud, D. Bouniol, A. J. Heymsfield, A. Bansemmer, P. R. A. Brown,
 1114 and R. M. Forbes, 2005: Statistical properties of the normalized ice particle size distribution. *J. Geophys.*
 1115 *Res.*, **110**, doi:10.1029/2004JD005405.
 1116
- 1117 Delanoë, J. M. E., A. J. Heymsfield, A. Protat, A. Bansemmer, and R. J. Hogan, 2014: Normalized
 1118 particle size distribution for remote sensing application. *J. Geophys. Res.*, **119**,
 1119 doi:10.1002/2013JD020700.
 1120
- 1121 Demortier, Luc, 1995: Assessing the Significance of a Deviation in the Tail of a Distribution.
 1122 Collider Detector at Fermilab note 3419.
 1123
- 1124 Field, P. R., 2000: Bimodal ice spectra in frontal clouds. *Quart. J. Roy. Meteor. Soc.*, **126**, 379-
 1125 392.
 1126
- 1127 Field, P. R., R. Wood, P. R. A. Brown, P. H. Kay, E. Hirst, R. Greenaway, and J. A. Smith,

1128 2003: Ice Particle Interarrival Times Measured with a Fast FSSP. *J. Atmos. Oceanic Technol.*, **20**, 249-
1129 261.

1130

1131 Field, P. R., R. J. Hogan, P. R. A. Brown, A. J. Illingworth, T. W. Choulaton, and R. J. Cotton,
1132 2005: Parameterization of ice-particle size distributions for mid-latitude stratiform cloud. *Quart. J. Roy.
1133 Meteor. Soc.*, **131**, 1997-2017.

1134

1135 Field, P. R., A. J. Heymsfield, and A. Bansemmer, 2006: Shattering and particle interarrival times
1136 measured by optical array probes in ice clouds. *J. Atmos. Oceanic Technol.*, **23**, 1357-1371.

1137

1138 [Fugal, J., and R. Shaw, 2009: Cloud particle size distributions measured with an airborne digital in-line holographic
1139 instrument. *Atmos. Meas. Tech.*, **2**, 259-271, doi:10.5194/amt-2-259-2009.](#)

1140

1141 [Garrett, T. J., H. Gerbert, D.G. Baumgardner, C.H. Twohy, and E.M. Weinstock, 2003: Small, highly reflective ice
1142 crystals in low-latitude cirrus. *Geophys. Res. Lett.*, **30**, doi:10.1029/2003GL018153.](#)

1143

1144 Gayet, J.-F., F. Auriol, A. Minikin, J. Stroem, M. Seifert, R. Krejci, A. Petzold, G.
1145 Febvre, and U. Schumann, 2002: Quantitative measurement of the microphysical and optical properties of
1146 cirrus clouds with four different in situ probes: Evidence of small ice crystals. *Geophys. Res. Lett.*, **29**,
1147 doi:10.1029/2001GL014342.

1148

1149 Gayet, J.-F., J. Ovarlez, V. Shcherbakov, J. Stroem, U. Schumann, A. Minikin, F. Auriol,
1150 A. Petzold, and M. Monier, 2004: Cirrus cloud microphysical and optical properties at southern and
1151 northern midlatitudes during the INCA experiment. *J. Geophys. Res.*, **109**, D20206,
1152 doi:10.1029/2004JD004803.

1153

1154 Gayet, J.-F., V. Shcherbakov, H. Mannstein, A. Minikin, U. Schumann, J. Stroem, A.
1155 Petzold, J. Ovarlez, and F. Immler, 2006: Microphysical and optical properties of midlatitude cirrus
1156 clouds observed in the southern hemisphere during INCA. *Quart. J. Roy. Meteor. Soc.*, **132**, 2719-2748.

1157

1158 [Gerber, H. and P. J. DeMott, 2014: Response of FSSP-100 and PVM-100A to Small Ice Crystals. *J. Atmos.
1159 Oceanic Technol.*, **31**, 2145-2155, doi:10.1175/JTECH-D-13-00228.1.](#)

1160

1161 Gurganus, C. and P. Lawson, 2016: Improvements in Optical Array Probe Characterization:
1162 Laboratory and Simulation Results. *XVII International Conference on Clouds and Precipitation*,
1163 Manchester, UK, the International Association of Meteorology and Atmospheric Sciences and the
1164 International Commission on Clouds and Precipitation.

1165

1166 Hammonds, K. D., G. G. Mace, and S. Y. Matrosov, 2014: Characterizing the Radar
1167 Backscatter-Cross-Section Sensitivities of Ice-Phase Hydrometeor Size Distributions via a Simple Scaling
1168 of the Clausius-Mossotti Factor. *J. Appl. Meteor. Climatol.*, **53**, 2761-2774.

1169

1170 [Heymsfield, A. J., and G. M. McFarquhar, 1996: High albedos of cirrus in the tropical Pacific warm pool:
1171 Microphysical interpretations from CEPEX and from Kwajalein, Marshall Islands. *J. Atmos. Sci.*, **53**,
1172 2424-2451, doi:10.1175/1520-0469\(1996\)053<2424:HAOCIT>2.0.CO;2.](#)

1173

1174 Heymsfield, A. J., A. Bansemmer, P. R. Field, S. L. Durden, J. L. Stith, J. E. Dye, W. Hall, and C.
1175 A. Grainger, 2002: Observations and Parameterizations of Particle Size Distributions in Deep Tropical
1176 Cirrus and Stratiform Precipitating Clouds: Results from In Situ Observations in TRMM Field Campaigns.
1177 *J. Atmos. Sci.*, **59**, 3457-3491.

1178

1179 Heymsfield, A. J., 2003: Properties of Tropical and Midlatitude Ice Cloud Particle Ensembles.
1180 Part I: Median Mass Diameters and Terminal Velocities. *J. Atmos. Sci.*, **60**, 2573-3591.

1181

1182 Heymsfield, A. J., A. Bansemmer, G. Heymsfield, and A. O. Fierro, 2009: Microphysics of
1183 Maritime Tropical Convective Uprrafts at Temperatures from -20° to -60°C. *J. Atmos. Sci.*, **66**, 3530-3562.

1184
1185 Heymsfield, A. J. C. Schmitt, A. Bansemer, and C. H Twohy, 2010: Improved representation of
1186 ice particle masses based on observations in natural clouds, *J. Atmos. Sci.*, **67**, 3303-3318,
1187 doi:10.1175/2010JAS3507.1
1188
1189 [Heymsfield, A.J., M. Krämer, A. Luebke, P. Brown, D.J. Cziczo, C. Franklin, P. Lawson, U. Lohmann, G.
1190 McFarquhar, Z. Ulanowski, and K. Van Tricht, 2017: Cirrus Clouds. *Meteorological Monographs*, **58**, 2.1–
1191 2.26, doi: 10.1175/AMSMONOGRAPHS-D-16-0010.1.](#)
1192
1193 Hobbs, P. V. and A. L. Rangno, 1985: Ice particle concentrations in clouds. *J. Atmos.*
1194 *Sci.*, **42**, 2523–2549.
1195
1196 Hogan, R. J., L. Tian, P. R. A. Brown, C. D. Westbrook, A. J. Heymsfield, and J. D. Eastment,
1197 2012: Radar Scattering from Ice Aggregates Using the Horizontally Aligned Oblate Spheroid
1198 Approximation. *J. Appl. Meteor. Climatol.*, **51**, 655-671.
1199
1200 Jackson, R. C. and G. M McFarquhar, 2014: An Assessment of the Impact of Antishattering
1201 Tips and Artifact Removal Techniques on Bulk Cloud Ice Microphysical and Optical Properties Measured
1202 by the 2D Cloud Probe. *J. Atmos. Oceanic Technol.*, **30**, 2131-2144.
1203
1204 Jackson, R. C., G. M. McFarquhar, J. Stith, M. Beals, R. A. Shaw, J. Jensen, J. Fugal, and A.
1205 Korolev, 2014: An Assessment of the Impact of Antishattering Tips and Artifact Removal Techniques on
1206 Cloud Ice Size Distributions Measured by the 2D Cloud Probe. *J. Atmos. Oceanic Technol.*, **31**, 2576-
1207 2590.
1208
1209 Jensen, E. J., and Coauthors, 2009: On the importance of small ice crystals in tropical anvil
1210 cirrus. *Atmos. Chem. Phys.*, **9**, 5519-5537.
1211
1212 Johnson, R. W., D. V. Kliche, and P. L. Smith, 2013: Maximum likelihood estimation
1213 of gamma parameters for coarsely-binned and truncated raindrop size data. *Quart. J. Roy. Meteor. Soc.*,
1214 doi:10.1002/qj.2209.
1215
1216 Khain, A., M. Pinsky, T. Elperin, N. Kleeorin, I. Rogachevskii, and A. Kostinski, 2007:
1217 Critical comments to results of investigations of drop collisions in turbulent clouds. *Atmospheric Research*,
1218 **86**, 1–20.
1219
1220 [Knollenburg, R., 1976: Three new instruments for cloud physics measurements: The 2-D spectrometer probe, the
1221 forward scattering spectrometer probe, and the active scattering aerosol spectrometer. Preprints, *Int. Conf.*
1222 *on Cloud Physics*, Boulder, CO, Amer. Meteor. Soc., 554-561.](#)
1223
1224 [Knollenburg, R., 1981: Techniques for probing cloud microstructure. *Clouds, Their Formation, Optical Properties*
1225 *and Effects*, P. V. Hobbs and A. Deepak, Eds., Academic Press, 15-91.](#)
1226
1227 Korolev, A. V. and G. Isaac, 2003: Roundness and Aspect Ratio of Particles in Ice Clouds. *J.*
1228 *Atmos. Sci.*, **60**, 1795-1808.
1229
1230 Korolev, A. V., E. F. Emery, J. W. Strapp, S. G. Cober, G. A. Isaac, M. Wasey, and D. Marcotte,
1231 2011: Small Ice Particles in Tropospheric Clouds: Fact or Artifact?. *Bull. Amer. Meteor. Soc.*, **92**, 967-
1232 973.
1233
1234 Korolev, A., E. Emery, and K Creelman, 2013a: Modification and Tests of Particle Probe Tips
1235 to Mitigate Effects of Ice Shattering. *J. Atmos. Oceanic Technol.*, **30**, 690-708.
1236
1237 Korolev, A. V., E. F. Emerty, J. W. Strapp, S. G. Cober, and G. A. Isaac, 2013b: Quantification
1238 of the effects of Shattering on Airborne Ice Particle Measurements. *J. Atmos. Oceanic Technol.*, **30**, 2527-
1239 2553.

1240
1241 Korolev, A., and P. R. Field, 2015: Assessment of the performance of the inter-arrival time
1242 algorithm to identify ice shattering artifacts in cloud particle probe measurements. *Atmos. Meas. Tech.*, **8**,
1243 761-777.
1244
1245 Kostinski, A. B., and R. A. Shaw, 2001: Scale-dependent droplet clustering in turbulent
1246 clouds. *J. Fluid. Mech.*, **434**, 389–398.
1247
1248 [Lance, S., C. A. Brock, D. Rogers, and J. A. Gordon, 2010: Water droplet calibration of the cloud droplet probe](#)
1249 [\(CDP\) and in-flight performance in liquid, ice and mixed-phase clouds during ARCPAC. *Atmos. Meas.*](#)
1250 [Tech.](#), **3**, 1683-1706, doi:10.5194/amt-3-1683-2010.
1251
1252 [Lawson, R. P., R. E. Stewart, and L. J. Angus, 1998: Observations and numerical simulations of the origin and](#)
1253 [development of very large snowflakes. *J. Atmos. Sci.*, **55**, 3209-3229, doi:10.1175/1520-](#)
1254 [0469\(1998\)055<3209:OANSOT>2.0.CO;2.](#)
1255
1256 Lawson, R. P., B. Baker, B. Pilson, and Q. Mo, 2006: In Situ Observations of the
1257 Microphysical Properties of Wave, Cirrus, and Anvil Clouds. Part II: Cirrus Clouds. *J. Atmos. Sci.*, **63**,
1258 3186-3203.
1259
1260 Lawson, R. P., E. Jensen, D. L. Mitchell, B. Baker, Q. Mo, and B. Pilson, 2010: Microphysical
1261 and radiative properties of tropical clouds investigated in TC4 and NAMMA. *J. Geophys. Res.*, **115**,
1262 doi:10.1029/2009JD013017.
1263
1264 Lawson, R. P., 2011: Effects of ice particles shattering on the 2D-S probe. *Atmos. Meas.*
1265 *Tech.*, **4**, 1361–1381.
1266
1267 Locatelli, J. D., and P. V. Hobbs, 1974: Fall speed and masses of solid precipitation particles. *J.*
1268 *Geophys. Res.*, **79**, 2185-2197.
1269
1270 MACPex Science Team, 2011: MACPEX. NASA Earth Science Project Office Data Archive, accessed 31 March
1271 2013. [Available online at <https://espoarchive.nasa.gov/archive/browse/macpex>.]
1272
1273 Matrosov, S. Y., 2007: Modeling Backscatter Properties of Snowfall at Millimeter Wavelengths.
1274 *J. Atmos. Sci.*, **64**, 1727-1736.
1275
1276 Matrosov, S. Y., G. G. Mace, R. Marchand, M. D. Shupe, A. G. Hallar, and I. B. McCubbin,
1277 2012: Observations of Ice Crystal Habits with a Scanning Polarimetric W-Band Radar at Slant Linear
1278 Depolarization Ratio Mode. *J. Atmos. Oceanic Technol.*, **29**, 989-1008.
1279
1280 McFarquhar, G. M., J. Um, M. Freer, D. Baumgardner, G. L. Kok, and G. Mace, 2007:
1281 Importance of small ice crystals to cirrus properties: Observations from the Tropical Warm Pool
1282 International Cloud Experiment (TWP-ICE). *Geophys. Res. Lett.*, **34**, doi:10.1029/2007GL029865.
1283
1284 Meakin, P., 1992: Aggregation kinetics. *Physica Scripta*, **46**, 295–331.
1285
1286 Mitchell, D. L., R. P. Lawson, and B. Baker, 2011: Understanding effective diameter and its
1287 application to terrestrial radiation in ice clouds. *Atmos. Chem. Phys.*, **11**, 3417-3429.
1288
1289 Moon, T. K., 1996: The Expectation-Maximization Algorithm. *IEEE Signal Processing*
1290 *Magazine*, **13**, 47-60.
1291
1292 Petty, G. W. and W. Huang, 2011: The Modified Gamma Size Distribution Applied to
1293 Inhomogenous and Nonspherical Particles: Key Relationships and Conversions. *J. Atmos. Sci.*, **68**, 1460-
1294 1473.
1295

1296 Pinsky, M. and A. Khain, 2003: Fine structure of cloud droplet concentration as seen
1297 from the Fast-FSSP measurements. Part II: Results of in situ observations. *J. Appl. Meteor. Climatol.*, **42**,
1298 65–73.
1299

1300 Posselt, D. and G. G. Mace, 2013: The Influence of Parameter Uncertainty on Snowfall
1301 Retrievals Using Markov Chain Monte Carlo Solution Methods. *J. Appl. Meteor. Climatol.*, Accepted.
1302

1303 Schwartz, M. C., 2014: Analysis of Cirrus Particle Size Distributions from Three In Situ Flight
1304 Campaigns: Applications to Cirrus Microphysics and Parameterization, Remote Sensing, and Radar
1305 Forward Model Simulators. Ph.D. dissertation, Dept. of Atmospheric Sciences, the University of Utah, 229
1306 pp.
1307

1308 SPartICus Science Team, 2010: SPartICus. Atmospheric Radiation Measurement Data Archive, PI/Campaign Data,
1309 accessed 26 March 2013. [Available online at
1310 <http://www.archive.arm.gov/discovery/#v/results/s/fiop::aaf2009Sparticus.>]
1311

1312 TC⁴ Science Team, 2007: TC4 DC-8 files. NASA Earth Science Project Office Data Archive, accessed 29 March
1313 2012. [Available online at <https://espoarchive.nasa.gov/archive/browse/tc4/DC8.>]
1314

1315 Tinel, C., J. Testud, J. Pelon, R. J. Hogan, A. Protat, J. Delanoë, and D. Bouniol, 2005:
1316 The retrieval of ice-cloud properties from cloud radar and lidar synergy. *J. Appl. Meteor.*, **44**, 860–875.
1317

1318 [Ulanowski, Z., P. H. Kaye, E. Hirst, R. S. Greenaway, R. J. Cotton, E. Hesse, and C. T. Collier, 2014: Incidence of](#)
1319 [rough and irregular atmospheric ice particles from Small Ice Detector 3 measurements. *Atmos. Chem.*](#)
1320 [Phys., **14**, 1649-1662, doi:10.5194/acp-14-1649-2014.](#)
1321

1322 Vidaurre, G. and J. Hallett, 2009: Particle Impact and Breakup in Aircraft Measurement. *J.*
1323 *Atmos. Oceanic Technol.*, **26**, 972-983.
1324

1324 Westbrook, C. D., R. C. Ball, P. R. Field, and A. J. Heymsfield, 2004a: Universality in
1325 snowflake aggregation. *Geophys. Res. Lett.*, **31**, L15104, doi:10.1029/2004GL020363.
1326

1327 Westbrook, C. D., R. C. Ball, P. R. Field, and A. J. Heymsfield, 2004b: Theory of growth by
1328 differential sedimentation, with application to snowflake formation. *Physical Review E*, **70**, 021403,
1329 doi:10.1103/PhysRevE.70.021403.
1330

1331 Wilks, D. S., 2006: *Statistical Methods in the Atmospheric Sciences*, 2nd Ed. Academic Press,
1332 627 pp.
1333

1334 Zhao, Y., G. G. Mace, and J. M. Comstock, 2011: The occurrence of particle size
1335 distribution bimodality in midlatitude cirrus as inferred from ground-based remote sensing data. *J. Atmos.*
1336 *Sci.*, **68**, 1162–1176.
1337

1338 **FIGURE CAPTIONS**

1339
1340 | [Figure 1: Flowchart illustrating the method of comparison between parameterized shatter-corrected 2DC/2DP dataset, uncorrected 2DC/2DP dataset, and shatter-corrected 2D-S dataset.](#)

1341
1342
1343 | Figure 2: Comparisons of computed and measured total number concentration for 15-second PSD averages and for
1344 truncation of none through the first two PSD size bins.

1345
1346 | Figure 3: Histograms of normalized PSDs from each flight campaign, overlaid with their mean, normalized PSDs
1347 (D05 normalization). The color map is truncated at 75% of the highest number of samples in a bin so as to increase
1348 contrast. (a) TC⁴ (b) MACPEX (c) SPaTICus (d) all data combined

1349 | Figure 4: The mean, normalized PSD (D05 normalization) from all three datasets combined, overlaid with two
1350 parameterizations from D05: the gamma-mu parameterization (dash-dotted curve) and the modified gamma
1351 parameterization (dashed curve). Panel (b) is a zoom-in on a portion of panel (a).

1352 | Figure 5: Same as Figure 3, but using D14 normalization.

1353 | Figure 6: The mean, normalized PSD (D14 normalization) from all three datasets combined, overlaid with the
1354 parameterizations from D14. Panel (b) is a zoom-in on a portion of panel (a).

1355
1356 | Figure 7: Total number concentration computed using the parameterized universal PSDs from D05 along with true
1357 values of N_0^* and D_m (from the 2D-S data) scattered vs. total number concentration computed directly from
1358 untransformed 2D-S data.

1359
1360 | Figure 8: Mean relative error and standard deviation of the relative error between total number concentration
1361 (divided by 10), effective radius, IWC, and Z as computed directly from the 2D-S and as computed from the
1362 modified-gamma universal PSD shape and the true N_0^* and D_m computed from the 2D-S data. [Standard error of
1363 the mean and standard deviation are shown with red error bars.](#)

1364
1365 | Figure 9: As in Figure 8, but using the shatter-corrected 2DC parameterization.

1366
1367
1368 | Figure 10: Data from TC⁴ alone. The mean, normalized PSD from the 2D-S is overlaid with the mean, normalized
1369 PSD obtained from combining the 2D-S with the PIP and the modified gamma parameterization from D05 (dashed
1370 curve). Panel (b) is a zoom-in on a portion of panel (a).

1371
1372 | Figure 11: Two-dimensional histogram of 94 GHz effective radar reflectivity computed, using the
1373 Hammonds/Matrosov approach, from the 2D-S alone versus that computed from the 2D-S combined with the PIP.

1374
1375 | Figure 12: Distributions of quantities computed using the parametric modified gamma distribution along with the
1376 true values of N_0^* and D_m computed from the 2D-S alone and from the 2D-S combined with the PIP. (a) N_T (b)
1377 extinction coefficient (c) IWC (d) 94 GHz effective radar reflectivity

1378
1379 | Figure 13: Marginal pdfs of quantities computed directly from 2D-S data, as well as computed using the
1380 parameterized 2D-S and the parameterized, uncorrected 2DC. (a) total number concentration (b) shortwave
1381 extinction coefficient (c) ice water content (d) radar reflectivity

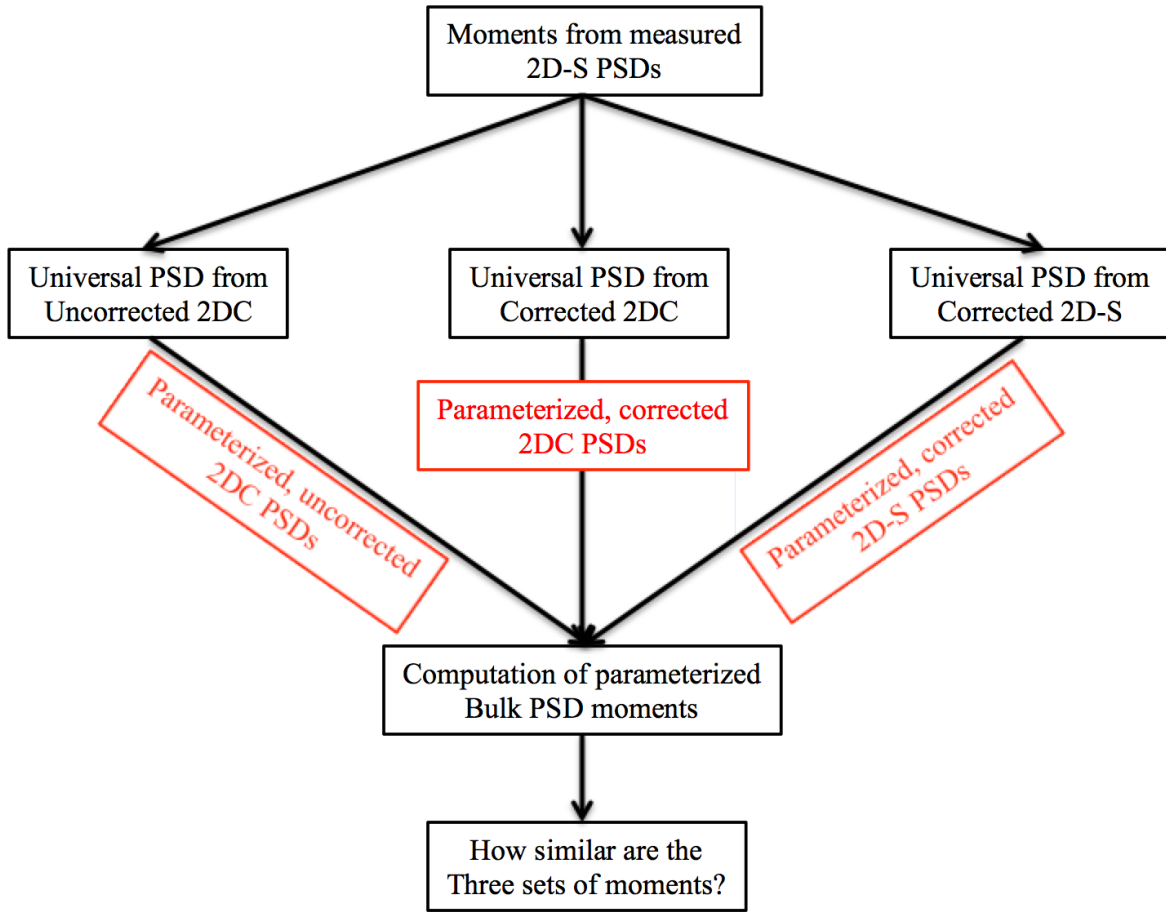
1382
1383 | Figure 14: Marginal pdfs of quantities computed directly from 2D-S data, as well as computed using the
1384 parameterized 2D-S and the parameterized, corrected 2DC. (a) total number concentration (b) shortwave extinction

1385

1386

1387
1388
1389

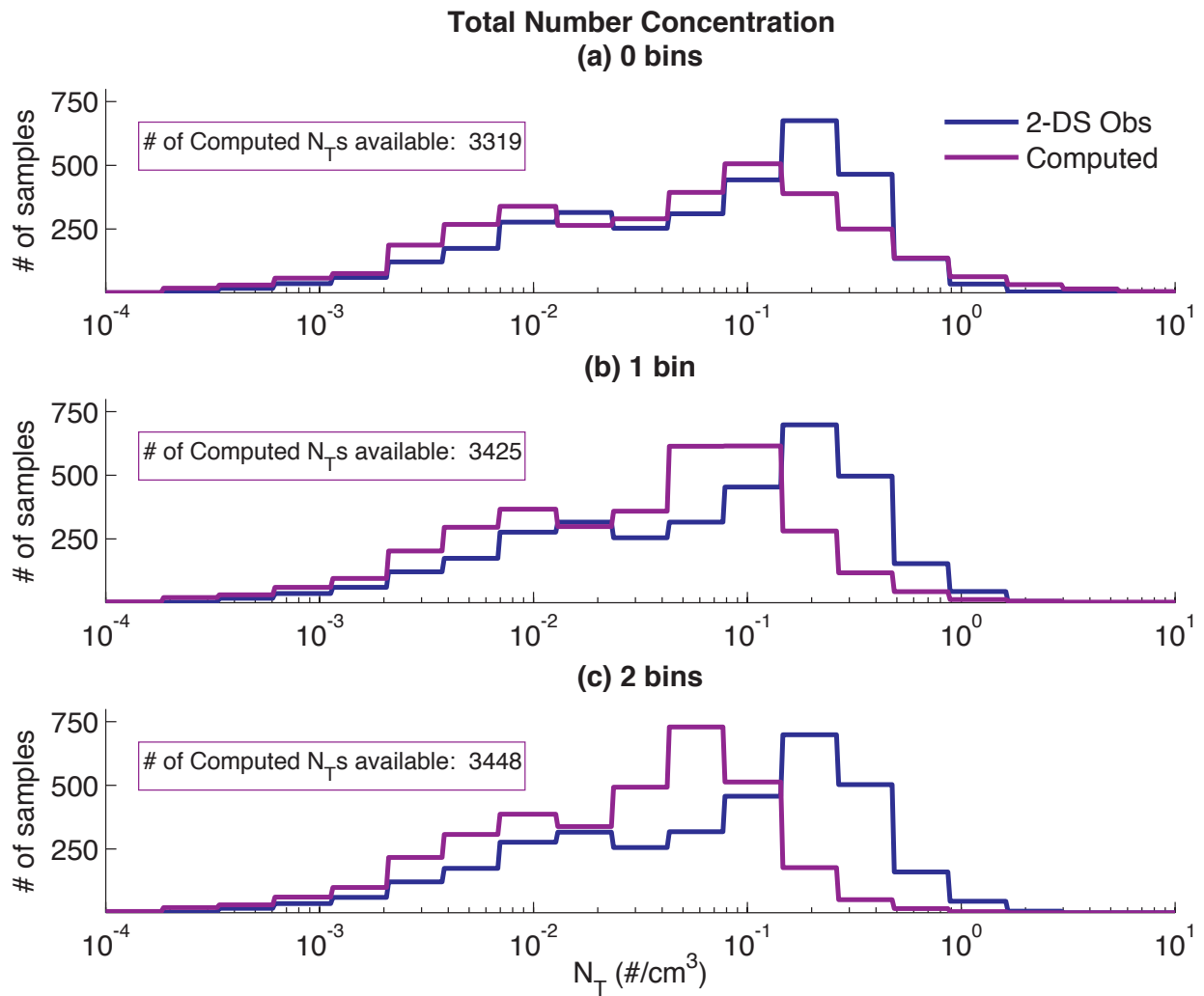
FIGURES



1390
1391
1392
1393

Figure 2: Flowchart illustrating the method of comparison between parameterized shatter-corrected 2DC/2DP dataset, uncorrected 2DC/2DP dataset, and shatter-corrected 2D-S dataset.

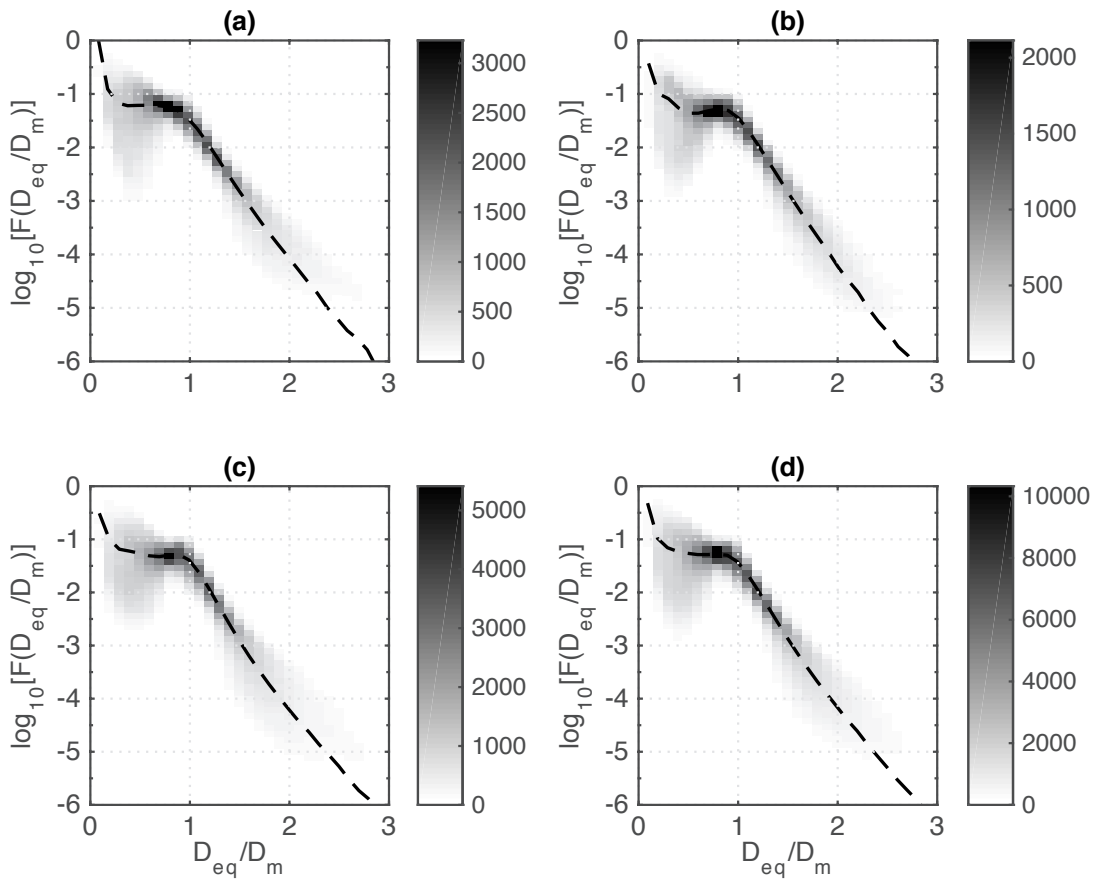
1394
1395
1396



1397
1398
1399

Figure 2: Comparisons of computed and measured total number concentration for 15-second PSD averages and for truncation of none through the first two PSD size bins.

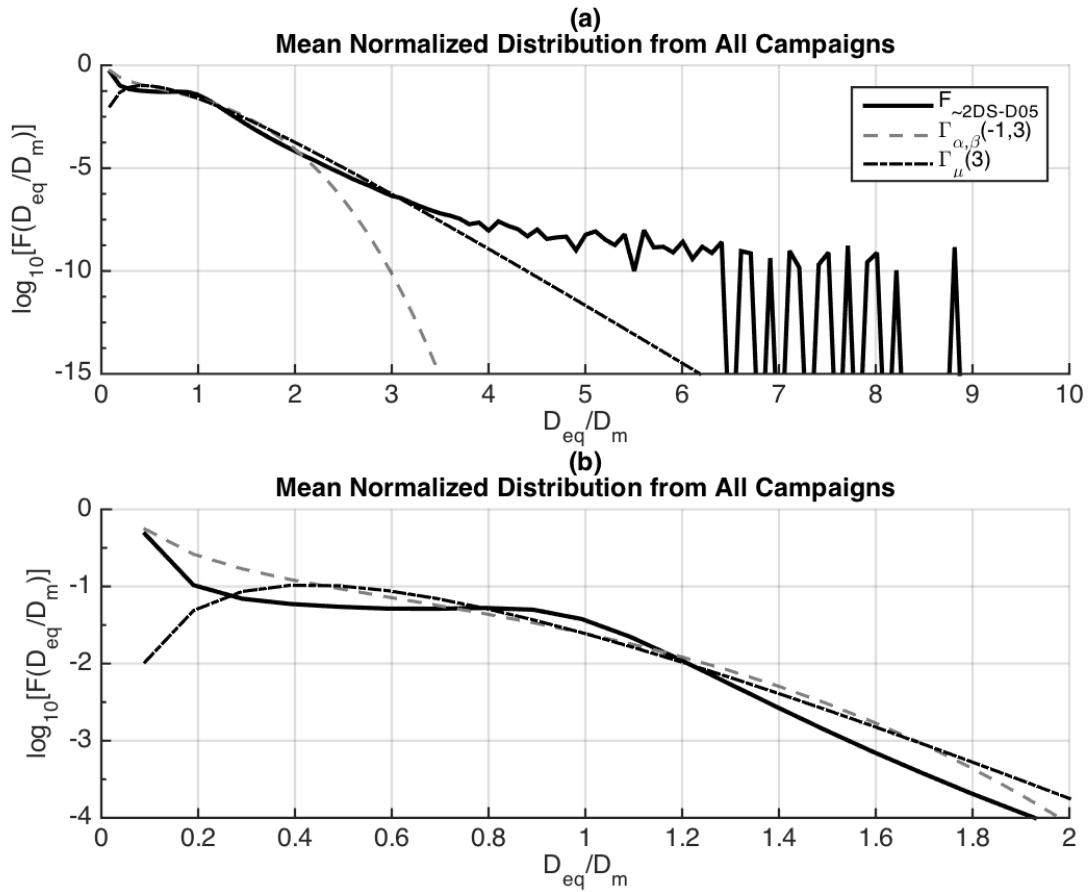
1400
1401



1402
 1403 |
 1404
 1405

Figure 3: Histograms of normalized PSDs from each flight campaign, overlaid with their mean, normalized PSDs (D05 normalization). The color map is truncated at 75% of the highest number of samples in a bin so as to increase contrast. (a) TC⁴ (b) MACPEX (c) SPARTICUS (d) all data combined

1406



1407
 1408 | **Figure 4:** The mean, normalized PSD (D05 normalization) from all three datasets combined, overlaid with
 1409 two parameterizations from D05: the gamma-mu parameterization (dash-dotted curve) and the modified
 1410 gamma parameterization (dashed curve). Panel (b) is a zoom-in on a portion of panel (a).

1411

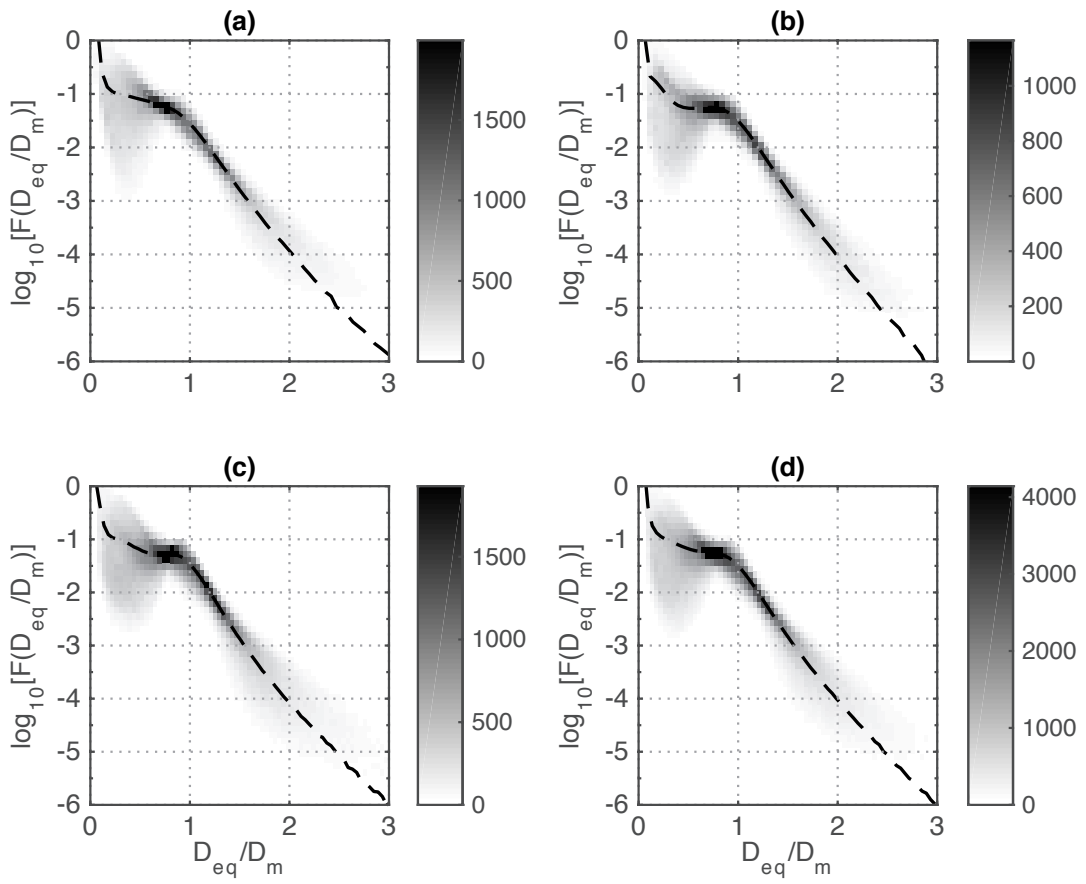
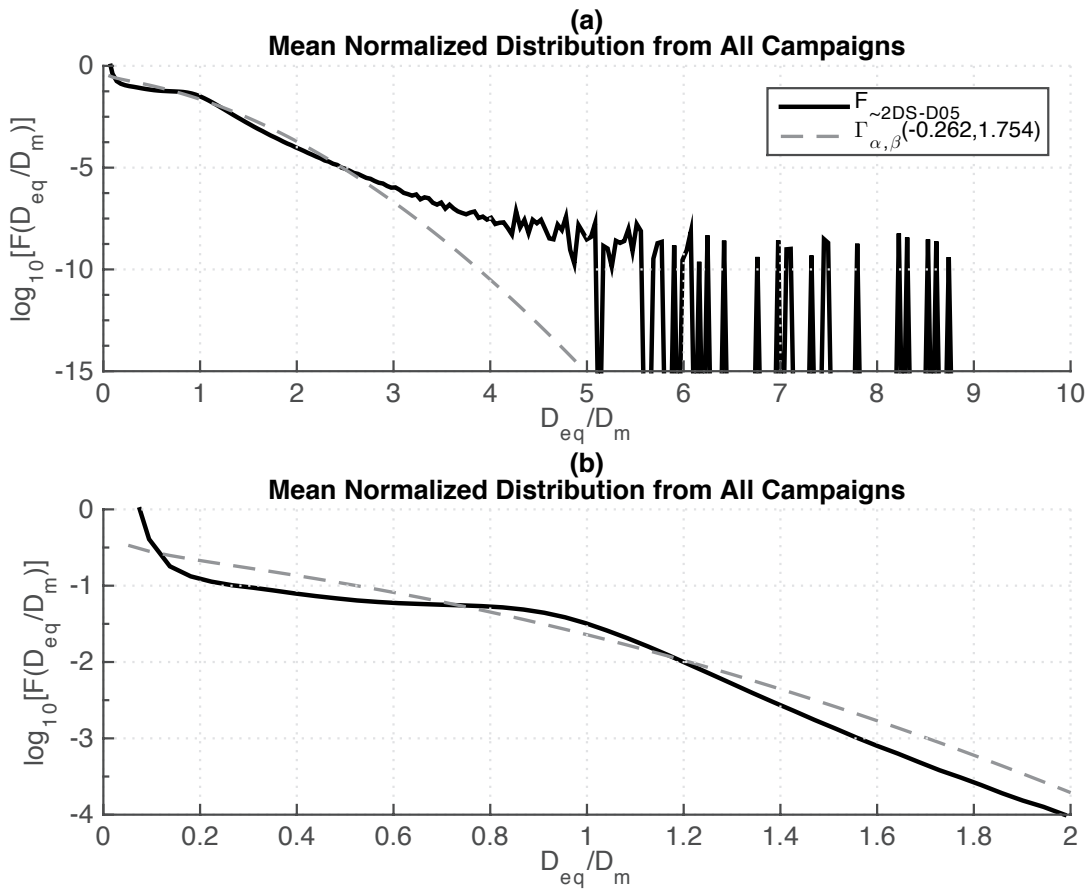


Figure 5: Same as Figure 3, but using D14 normalization.

1412
1413

1414
1415
1416

1417



1418

1419

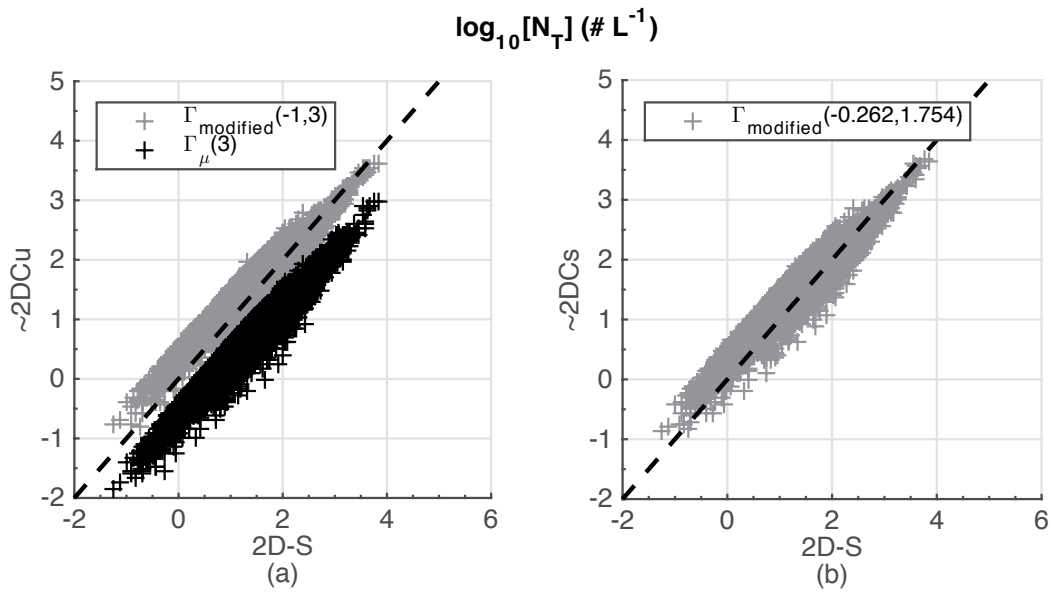
1420

Figure 6: The mean, normalized PSD (D14 normalization) from all three datasets combined, overlaid with the parameterizations from D14. Panel (b) is a zoom-in on a portion of panel (a).

1421

1422

1423



1424

1425

Figure 7: Total number concentration computed using the parameterized universal PSDs from D05 along with true values of N_0^* and D_m (from the 2D-S data) scattered vs. total number concentration computed directly from untransformed 2D-S data.

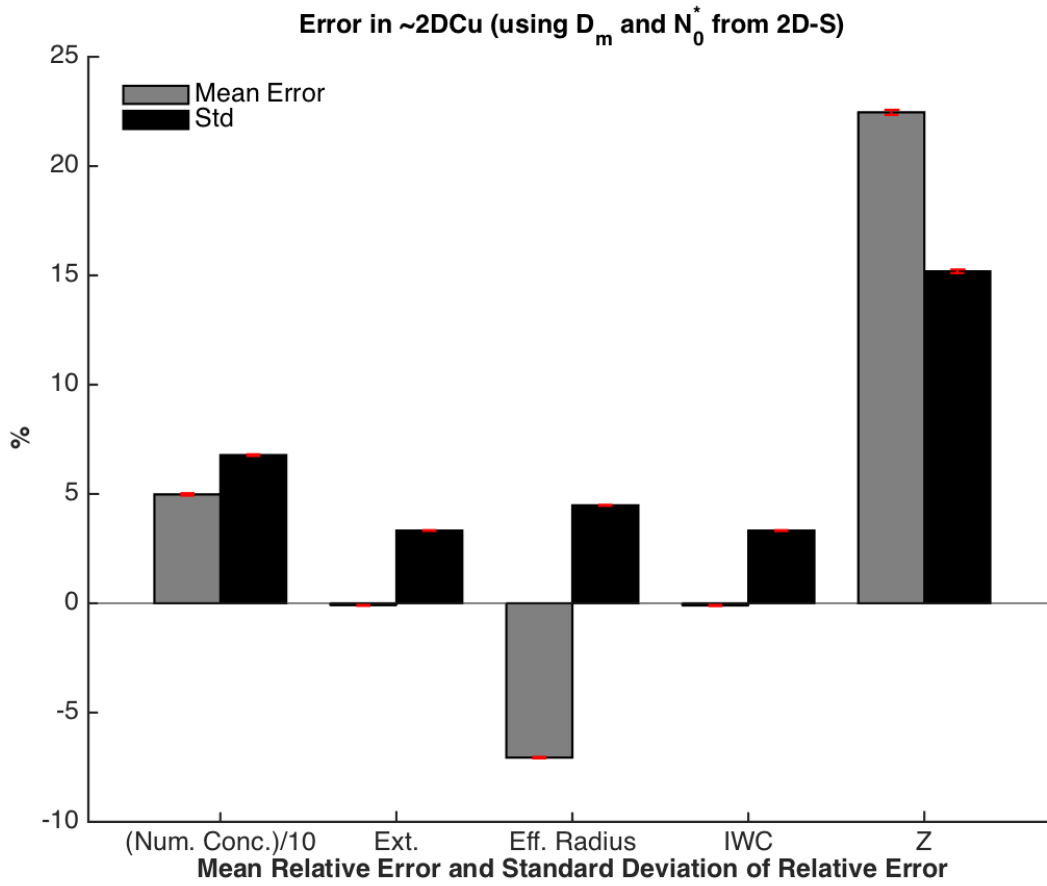
1426

1427

1428

1429

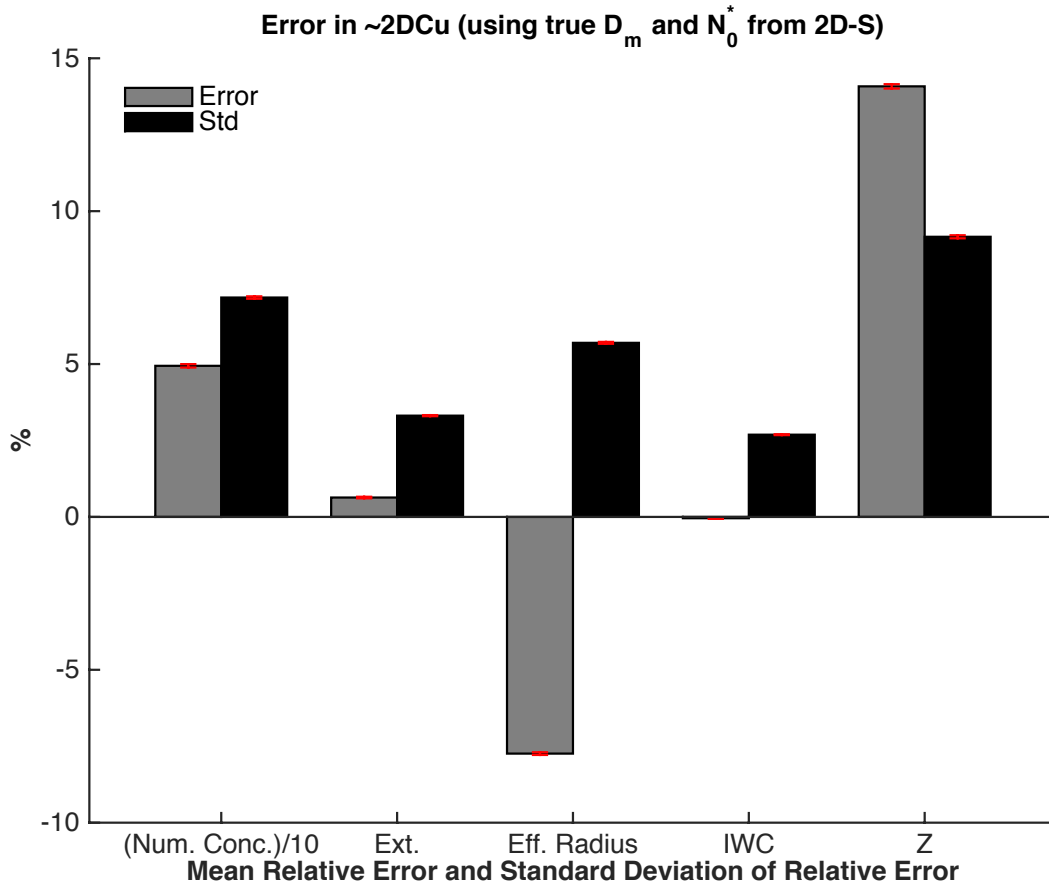
1430



1431
1432
1433
1434
1435
1436

Figure 8: Mean relative error and standard deviation of the relative error between total number concentration (divided by 10), effective radius, IWC, and Z as computed directly from the 2D-S and as computed from the modified-gamma universal PSD shape and the true N_0^* and D_m computed from the 2D-S data. Standard error of the mean and standard deviation are shown with red error bars.

1437



1438

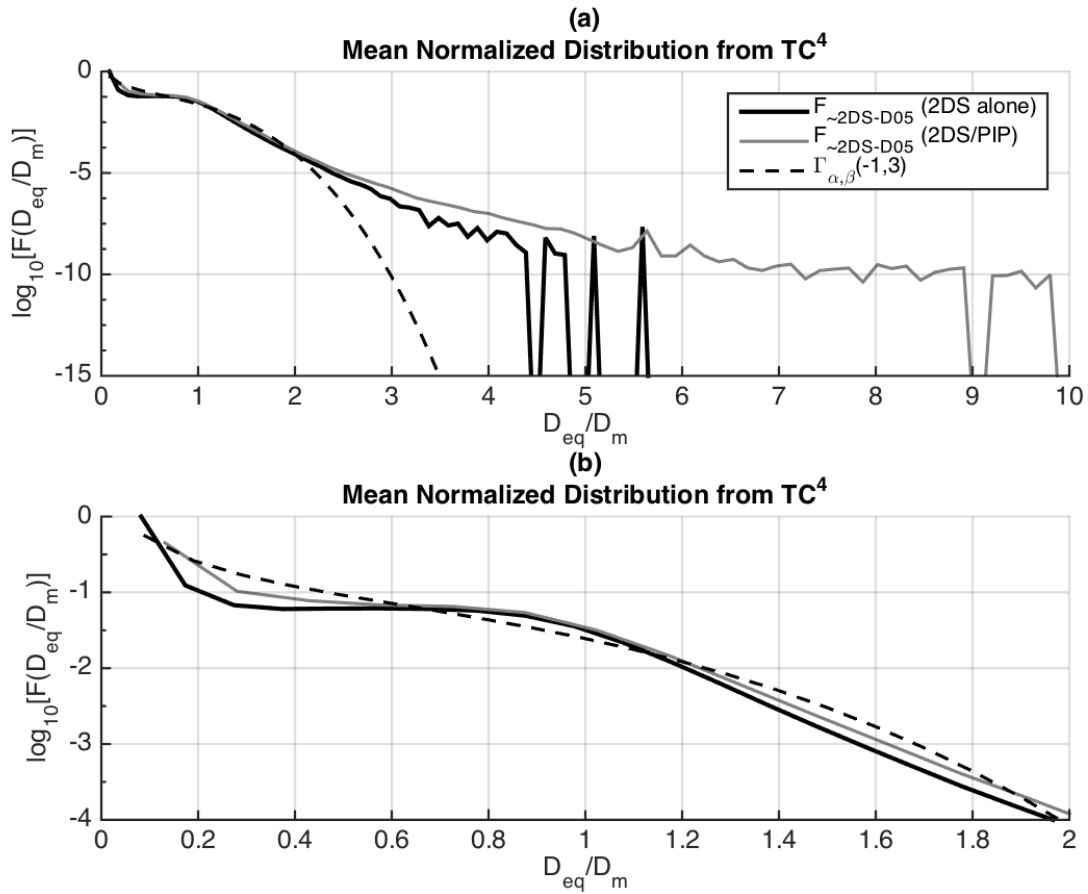
1439

Figure 9: As in Figure 8, but using the shatter-corrected 2DC parameterization.

1440

1441

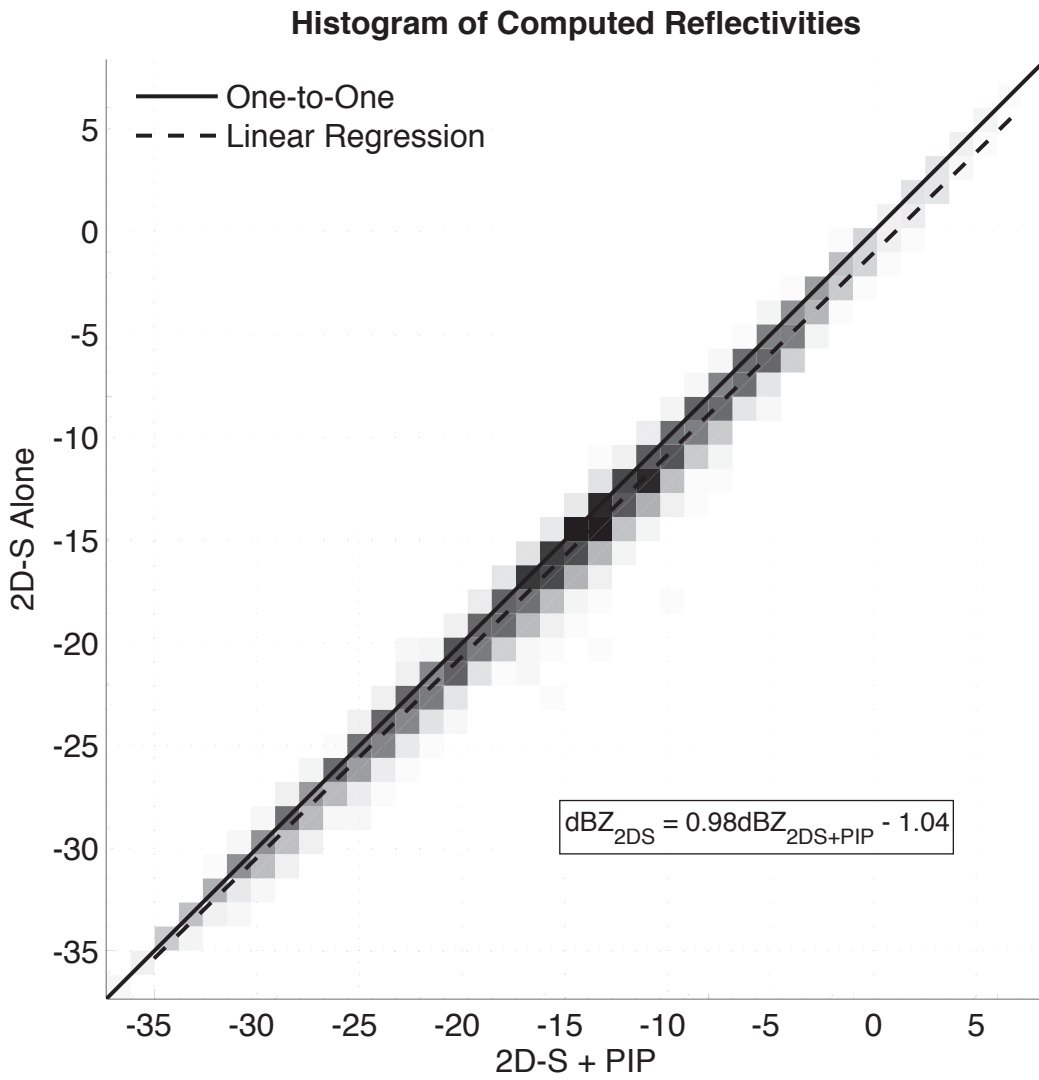
1442
1443



1444
1445
1446
1447

Figure 10: Data from TC⁴ alone. The mean, normalized PSD from the 2D-S is overlaid with the mean, normalized PSD obtained from combining the 2D-S with the PIP and the modified gamma parameterization from D05 (dashed curve). Panel (b) is a zoom-in on a portion of panel (a).

1448



1450

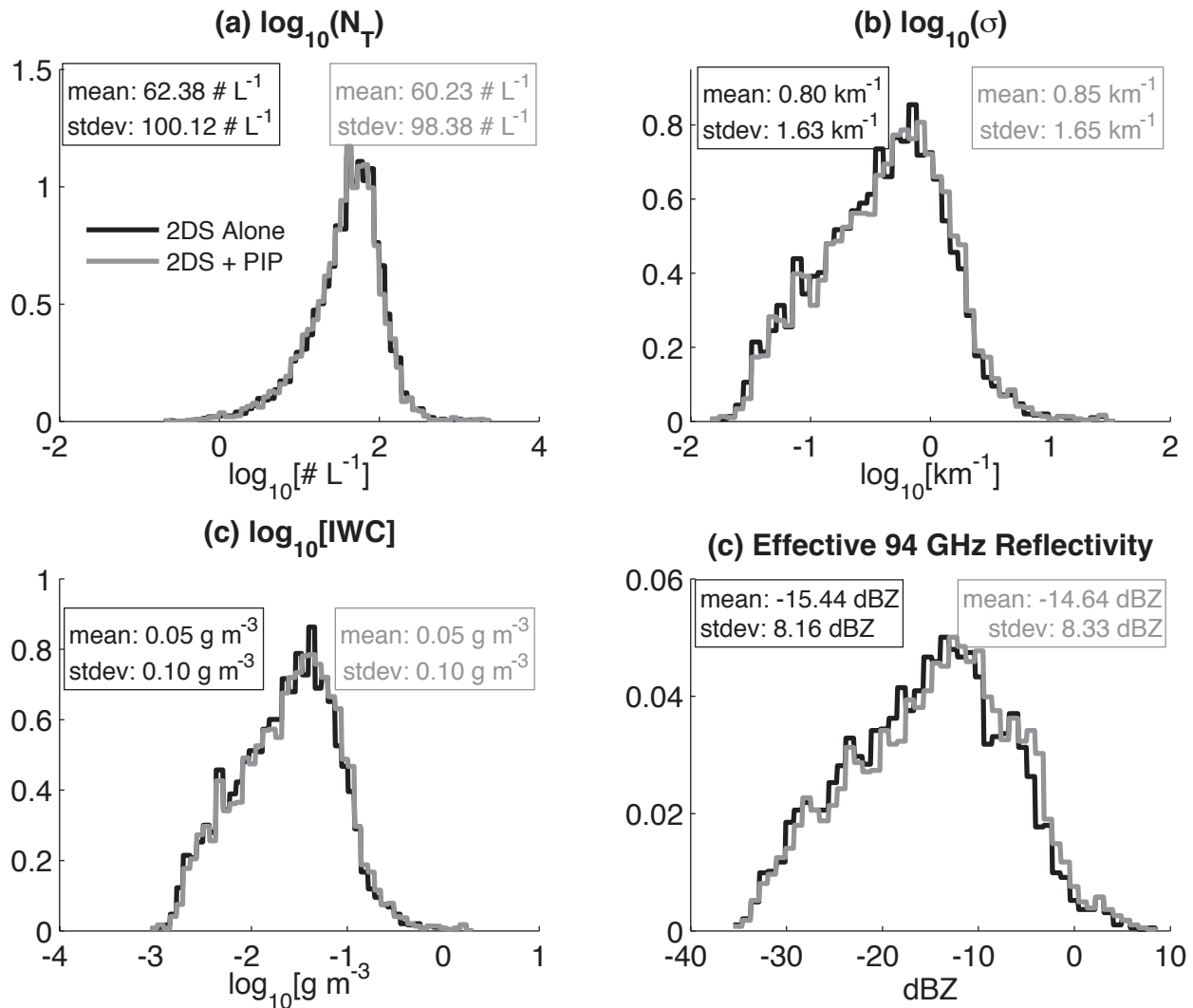
1451 |

1452

1453

Figure 11: Two-dimensional histogram of 94 GHz effective radar reflectivity computed, using the Hammonds/Matrosov approach, from the 2D-S alone versus that computed from the 2D-S combined with the PIP.

1454



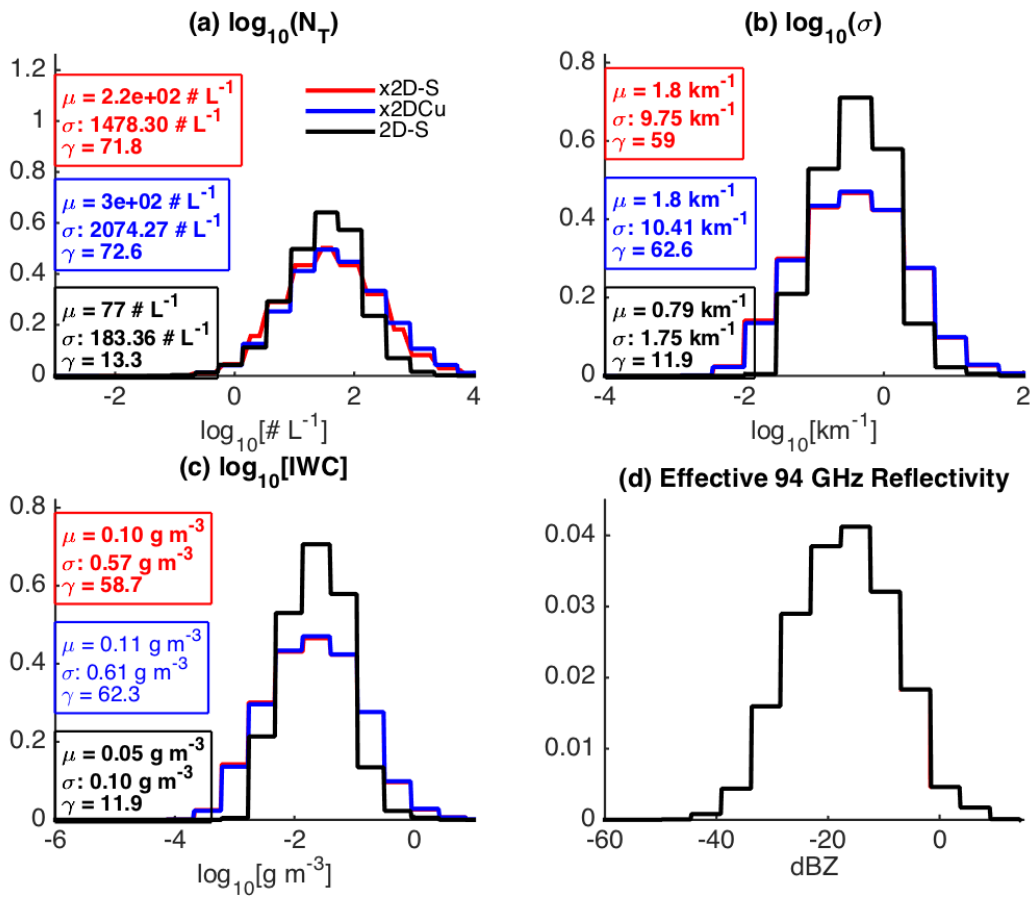
1455

1456 | **Figure 12:** Distributions of quantities computed using the parametric modified gamma distribution along
 1457 with the true values of N_0^* and D_m computed from the 2D-S alone and from the 2D-S combined with the
 1458 PIP. (a) N_T (b) extinction coefficient (c) IWC (d) 94 GHz effective radar reflectivity

1459

1460

1461



1463

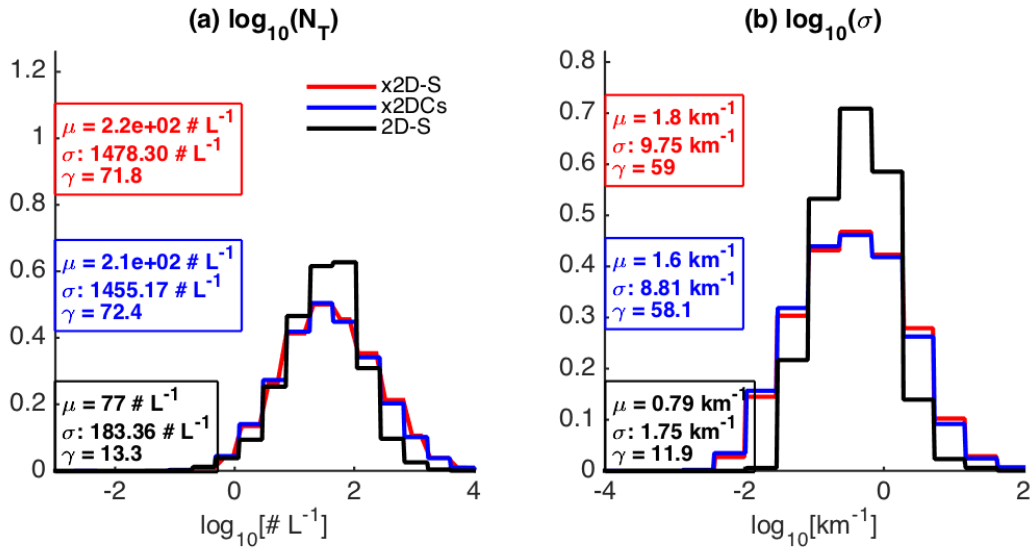
1464

1465

1466

Figure 13: Marginal pdfs of quantities computed directly from 2D-S data, as well as computed using the parameterized 2D-S and the parameterized 2DC. (a) total number concentration (b) shortwave extinction coefficient (c) ice water content (d) radar reflectivity

1467



1469
 1470
 1471
 1472

Figure 14: Marginal pdfs of quantities computed directly from 2D-S data, as well as computed using the parameterized 2D-S and the parameterized, corrected 2DC. (a) total number concentration (b) shortwave extinction